A&A 494, 443–460 (2009)
DOI: 10.1051/0004-6361:200809617

Astronomy & Astrophysics

The great observatories origins deep survey

VLT/VIMOS spectroscopy in the GOODS-south field

P. Popesso[1], M. Dickinson[4], M. Nonino[3], E. Vanzella[2,3], E. Daddi[8], R. A. E. Fosbury[5], H. Kuntschner[5], V. Mainieri[7], S. Cristiani[3], C. Cesarsky[7], M. Giavalisco[6], A. Renzini[2], and the GOODS Team

[1] Max-Planck-Institut fur extraterrestrische Physik,, Giessenbachstrasse 2, 85748 Garching, Germany
e-mail: popesso@mpe.mpg.de
[2] Dipartimento di Astronomia dell'Università di Padova, Vicolo dell'Osservatorio 2, 35122 Padova, Italy
[3] INAF – Osservatorio Astronomico di Trieste, Via G.B. Tiepolo 11, 40131 Trieste, Italy
[4] National Optical Astronomy Obs., PO Box 26732, Tucson, AZ 85726, USA
[5] ST-ECF, Karl-Schwarzschild Str. 2, 85748 Garching, Germany
[6] Space Telescope Science Institute, 3700 San Martin Drive, Baltimore, MD 21218, USA
[7] European Southern Observatory, Karl-Schwarzschild-Strasse 2, Garching, 85748, Germany
[8] Université Paris-Sud 11, 15 rue Georges Clemenceau, 91405 Orsay, France⋆

Received 20 February 2008 / Accepted 14 November 2008

ABSTRACT

Aims. We present the first results from the VIsible Multiobject Spectrograph (VIMOS) ESO/GOODS program of spectroscopy for faint galaxies in the Chandra Deep Field South (CDF-S). This program complements the FORS2 ESO/GOODS campaign.
Methods. All 3312 spectra were obtained in service mode with VIMOS at the ESO/VLT UT3. The VIMOS LR-Blue and MR grisms were used to cover different redshift ranges. Galaxies at $1.8 < z < 3.5$ were observed in the GOODS VIMOS-LR-Blue campaign. Galaxies at $z < 1$ and Lyman Break Galaxies at $z > 3.5$ were observed in the VIMOS MR survey.
Results. Here we report results for the first 12 masks (out of 20 total). We extracted 2344 from 6 LR-Blue masks and 968 from 6 MR masks. A large percentage, 33% of the LR-Blue and 18% of the MR spectra, are serendipitous observations. We obtained 1481 and 656 redshifts in the LR-Blue and MR campaign, respectively, for a total success rate of 70% and 75%, respectively, which decrease to 63% and 68% when also the serendipitous targets are considered. The typical redshift accuracy is $\sigma_z = 0.001$. The reliability of the redshift estimate varies with the quality flag. The LR-Blue quality flag A redshifts are reliable at ∼95% confidence level, flag B redshifs at ∼70% and quality C et ∼40%. The MR redshift reliability is somewhat higher: 100% for quality flag A, ∼90% for quality flag B and ∼70% for flag C. By complementing our VIMOS spectroscopic catalog with all existing spectroscopic redshifts publicly available in the CDF-S, we created a redshift master catalog. By comparing this redshift compilation with different photometric redshift catalogs we estimate the completeness level of the CDF-S spectroscopic coverage in several redshift bins.
Conclusions. The completeness level is very high, >60%, at $z < 3.5$, and it is very uncertain at higher redshift. The master catalog was used also to estimate completeness and contamination levels of different galaxy photometric selection techniques. The BzK selection method leads to a ∼86% complete sample of $z > 1.4$ galaxies at $i_{AB} < 25$ mag and with a contamination ∼23% of lower redshift objects. The so-called "sub"-U-dropout and the U-dropout methods lead to an 80% complete galaxy sample at $z > 1.4$ and $i_{AB} < 25$ mag, with ∼24% low redshift contaminants.

Key words. cosmology: observations – cosmology: large-scale structure of Universe – galaxies: evolution

1. Introduction

The Great Observatories Origins Deep Survey (GOODS) is a public, multi-facility project that aims at answering some of the most profound questions in cosmology: how did galaxies form and assemble their stellar mass? When was the morphological differentiation of galaxies established and how did the Hubble sequence form? How did AGN form and evolve, and what role do they play in galaxy evolution? How much do galaxies and AGN contribute to the extragalactic background light? A project of this scope requires large and coordinated efforts from many facilities, pushed to their limits, to collect a database with sufficient quality and size for the task at hand. It also requires that the data be readily available to the worldwide community for independent analysis, verification, and follow-up.

The program targets two carefully selected fields, the Hubble Deep Field North (HDF-N) and the Chandra Deep Field South (CDF-S), with three NASA Great Observatories (HST, Spitzer and Chandra), ESA's XMM-Newton, and a wide variety of ground-based facilities. The area common to all the observing programs is 320 arcmin^2, equally divided between the North and South fields. For an overview of GOODS, see Dickinson et al. (2003), Renzini et al. (2003) and Giavalisco et al. (2004).

Spectroscopy is essential to reach the scientific goals of GOODS. Reliable redshifts provide the time coordinate needed to delineate the evolution of galaxy masses, morphologies, clustering, and star formation. They calibrate the photometric redshifts that can be derived from the imaging data at 0.36−8 μm. Spectroscopy will measure physical diagnostics for galaxies in the GOODS field (e.g., emission line strengths and ratios to trace

⋆ Based on observations made at the European Southern Observatory, Paranal, Chile (ESO program 171.A-3045 *The Great Observatories Origins Deep Survey: ESO Public Observations of the SIRTF Legacy/HST Treasury/Chandra Deep Field South.*)

star formation, AGN activity, ionization, and chemical abundance; absorption lines and break amplitudes that are related to the stellar population ages). Precise redshifts are also indispensable to properly plan for future follow-up at higher dispersion, e.g., to study galaxy kinematics or detailed spectral-line properties.

The ESO/GOODS spectroscopic program is designed to observe all galaxies in the CDF-S field for which VLT optical spectroscopy is likely to yield useful data. The program is organized in two campaigns, carried out at VLT/FORS2 at UT1 and VLT/VIMOS at UT3. The program makes full use of the VLT instrument capabilities, matching targets to instrument and disperser combinations in order to maximize the effectiveness of the observations.

The FORS2 campaign is now completed (Vanzella et al. 2005, 2006, 2008). 1715 spectra of 1225 individual targets have been observed and 887 redshifts have determined as a result. Galaxies have been selected adopting three different color criteria and using photometric redshifts. The resulting redshift distribution typically spans two redshift domains: from $z = 0.5$ to 2 and $z = 3$ to 6.5. The reduced spectra and the derived redshifts have been released to the community through the ESO web pages http://archive.eso.org/cms/eso-data/data-packages. The typical redshift uncertainty is estimated to be $\sigma_z \sim 0.001$.

We have carried out the VIMOS ESO/GOODS spectroscopic survey to complement the observations done with the FORS2 instrument, in order to ensure optimal completeness and sky coverage. The FORS2 campaign was designed to take advantage of that instrument's very high throughput at red wavelengths. This was particularly important for detecting rest-frame optical and near-ultraviolet spectral features (such as the [OII]3727 Å emission line) out to $z \approx 1.6$, and rest-frame UV emission and absorption lines at $z > 4$. The GOODS VIMOS campaign, in turn, takes advantage of that instrument's very large field of view and multiplexing capability, and its good instrumental throughput at roughly 360−900 nm. This enables us to measure large numbers of redshifts at $z < 1.4$ from the [OII]3727 Å emission line and other optical and near-UV features, as well as redshifts at $1.5 < z < 3.5$ from Lyman α emission and rest-frame UV absorption lines. The cumulative source counts on the CDF-S field taken from the deep public FORS1 data (Szokoly et al. 2004), show that down to $V_{AB} = 25$ mag there are ∼6000 objects over the 160 arcmin^2 of the GOODS field. The high multiplexing capabilities of VIMOS at VLT make it possible to reach the desired redshift completeness in a reasonable amount of observing time.

The GOODS VIMOS program used two different observational configurations, with different object selection criteria for each. Observations with the Medium Resolution (MR) orange grism target galaxies in the redshift ranges $0.5 < z < 1.3$ (primarily from [OII]) and $z > 3.5$ (from Ly α). Observations with the low resolution blue (LR-Blue) grism cover the wavelengths of Ly α and UV rest-frame absorption lines at $1.8 < z < 3.5$, a range not covered by the FORS2 spectroscopy. On average, ∼330 objects at a time have been observed with the low resolution ($R \sim 250$) blue grism and ∼140 with the medium resolution ($R \sim 1000$) orange grism. The overall goal of the GOODS spectroscopic campaign was to reach signal-to-noise ratios adequate for measuring redshifts for galaxies with AB magnitudes in the range ∼24−25, in the B-band for objects observed with the VIMOS LR-Blue grism, in the R-band for objects observed with the VIMOS MR grism, and in the z-band for objects observed with FORS2.

In this paper we report on the first 60% of the VIMOS spectroscopic follow-up campaign in the Chandra Deep Field South (CDF-S), carried out with the VIMOS instrument at the VLT from ESO observing periods P74 through P78 (mid-2004 through early 2007). 10 masks have been observed in the LR-Blue grism and 10 with the MR grism. Here we report results for the first 6 masks that have been analyzed from each of the LR-Blue and MR grisms.

The paper is organized as follows: in Sect. 2 we describe the survey strategy and in Sect. 3 the observations and the data reduction. The details of the redshift determination is presented in Sect. 4. In Sect. 5 we discuss the data and in Sect. 6 the reliability of the photometric techniques used to identify the high redshift targets. In Sect. 7 we present our the conclusions. Throughout this paper the magnitudes are given in the AB system ($AB \equiv 31.4-2.5 \log\langle f_\nu/\mathrm{nJy}\rangle$), and the ACS $F435W$, $F606W$, $F775W$, and $F850LP$ filters are denoted hereafter as B_{435}, V_{606}, i_{775} and z_{850}, respectively. We assume a cosmology with $\Omega_{\rm tot}, \Omega_M, \Omega_\Lambda = 1.0, 0.3, 0.7$ and $H_0 = 70$ km s^{-1} Mpc^{-1}.

2. The survey strategy

2.1. The VIMOS instrument

The VIsible MultiObject Spectrograph (VIMOS) is installed on the ESO/VLT, at the Nasmyth focus of the VLT/UT3 "Melipal" (Le Fevre et al. 2003). VIMOS is a 4-channel imaging spectrograph, each channel (a "quadrant") covering ∼7×8 arcmin^2 for a total field of view (a "pointing") of ∼218 arcmin^2. Each channel is a complete spectrograph, using either broad band filters for direct imaging, or $\sim 30 \times 30$ cm^2 slit masks at the entrance focal plane and grisms to disperse spectra onto 2048×4096 pixels^2 EEV CCDs.

The pixel scale is 0.205 arcsec/pixel, providing excellent sampling of the Paranal mean image quality and Nyquist sampling for a slit width of 0.5 arcsec. The spectra resolution ranges from ∼200 to ∼5000. Because of the large field of view of the instrument ($16' \times 18'$) and the lack of an atmospheric dispersion compensator, observations are restricted to 1.1 airmasses to minimize the loss of light due to atmospheric refractions.

In the MOS mode of observations, short "pre-images" are taken ahead of the observing run. Sources from a user-supplied catalog of targets are identified with objects in the pre-images in order to map the celestial coordinates of the observer's targets to the instrumental coordinate system. The slit masks are then prepared using the VMMPS tool, provided by ESO, with an automated optimization of slit number and position (see Bottini et al. 2005).

2.2. The field coverage: VIMOS pointing layout

The VIMOS geometry ($16' \times 18'$, with a cross gap of $2'$ between the quadrants) is such that only 50% of its instantaneous field of view can overlap with the $10' \times 16'$ region that roughly defines the GOODS-CDFS field. At least 3 VIMOS pointings are required to cover the whole GOODS area (see Fig. 1), filling the gaps between the spectrograph quadrants, and some fraction of the VIMOS coverage will fall outside the nominal GOODS area. The VIMOS multiplex allows observations to target an average of ∼360 objects per pointing in the case of the Low Resolution (LR) grism and ∼150 objects in the case of the Medium Resolution (MR) grism. Before the program began, we estimated that 10 Low Resolution and 10 Medium Resolution masks (on average 3 LR and 3 MR masks per pointing) would

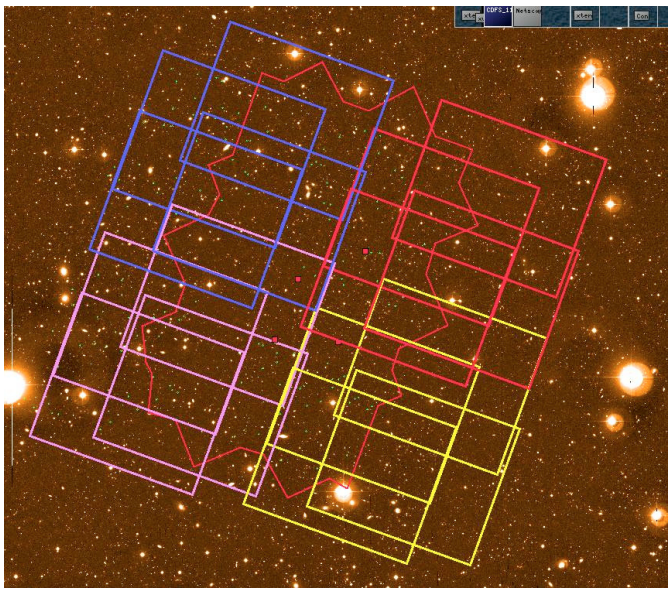

Fig. 1. Example of the VIMOS field coverage of the GOODS area in the CDF-S. Only three pointings from the VIMOS-MR campaign are shown for clarity. Each color indicates the position of one instrument quadrant in the three different pointings.

be needed to achieve ∼96% completeness in the spectroscopic coverage of ∼6000 targets. With an average integration time of 4 h per mask and 30% overheads, the observations therefore required a total of 125 h.

2.3. Target selection

Several categories of object selection criteria were used to ensure a sufficiently high density of target candidates on the sky to efficiently fill out multi-slit masks. Different criteria were used for the low resolution "LR-Blue" grism and the medium resolution "MR Orange" grism, based on the wavelength coverage of each instrumental configuration and the redshift ranges expected for the targeted objects. In general, the target selection strategy was designed to take advantages of VIMOS' strengths (very large multiplex, and the comparative blue sensitivity of the LR-B grism) and to complement those of other instruments being used in the overall GOODS spectroscopic effort (e.g., the high red throughput of FORS2). The VIMOS selection criteria were adjusted over the course of the multi-year observing campaign to optimize the survey success rate. Target catalogs were updated as the available GOODS imaging and photometric data improved (e.g., as the HST/ACS campaign was completed, and as VLT/ISAAC imaging coverage expanded concurrent with the spectroscopic campaign). The target lists were also updated to take into account partial results of this and other spectroscopic surveys (e.g., GOODS/FORS2, VVDS).

For the portion of the VIMOS field of view that overlaps the GOODS-S area proper, targets were selected for observation mainly using photometry from the GOODS-S HST/ACS and VLT/ISAAC imaging, as well as CTIO 4 m/MOSAIC U-band imaging. Slits outside the ACS and ISAAC coverage were populated by targets (mainly U-dropout and "sub-U-dropout" Lyman break galaxies) selected using ground-based optical data, primarily $BVRI$ imaging from the ESO 2.2 m WFI and U-band data from the CTIO 4 m. We summarize here the imaging data, source catalogs, and the main selection criteria used during the GOODS VIMOS survey in ESO observing periods P74-P78:

- CTIO 4 m MOSAIC U-band imaging and ESO 2.2 m WFI B- and R-band imaging, covering the $30' \times 30'$ "Extended" CDF (ECDFS), with AB magnitude 5σ depths 26, 26.2 and 25.8 mag, respectively (Giavalisco et al. 2004), used for Lyman break U-dropout and "sub-U-dropout" color selection, both inside and outside the nominal GOODS-S area. Source detection was done in the R-band image, and colors were measured through matched apertures in each band using data whose point spread functions were matched to achieve common angular resolution. The WFI R-band catalog also served as the primary astrometric reference catalog for mask design, and to define R-band magnitude limits for all samples targeted with VIMOS;
- HST-ACS B435 (B-band) and F850LP (z-band) imaging, covering the GOODS-S field (approximately 165 arcmin^2) with depth 27.8 and 27.4 mag (Giavalisco et al. 2004), used for the BzK color-selection technique within GOODS-S proper;
- VLT-ISAAC K_s-band imaging covering the GOODS-S field with depth 25.1 mag (Retzlaff et al. in preparation), for applying the BzK selection technique in GOODS-S field. Source detection was done in a mosaic of the ISAAC K_s images, and photometry colors were measured through matched apertures on binned mosaics of the HST/ACS images, degraded to match the PSF of the ISAAC data;
- Chandra Deep Field South X-ray catalog (Giacconi et al. 2002; Lehmer et al. 2005), covering an area somewhat larger than GOODS-S, with approximate sensitivity 2×10^{-16} erg cm^{-2} s^{-1} (in detail, varying with distance from the Chandra aim point at the field center).

The VIMOS LR-Blue grism covers the wavelength range 3500–6900 Å. Hence it is suitable for the observation of ultraviolet absorption and emission features of objects in the redshift range $1.8 \leq z \leq 3.8$. Targets for the low resolution campaign were selected using the following criteria:

- U-dropouts: Lyman break color selection of galaxies using the CTIO U and WFI B and R photometry. See Sect. 6 and Lee et al. (2006) for a detailed description of the selection criteria. This method was applied over the whole VIMOS area, both inside and outside the GOODS-S region proper. These criteria are designed to select blue, star-forming galaxies at $z \approx 3$;
- so-called "sub-U-dropouts": UBR color-selected objects with $U - B$ colors somewhat bluer than those of the normal $z \sim 3$ U-dropout Lyman break selection criteria, similar to "BX" selection criterion of Adelberger et al. (2004); see Sect. 6 for the detailed description of the selection criteria. These criteria are designed to select star-forming galaxies at somewhat lower redshifts than those of the regular U-dropouts, nominally $z \approx 1.8$ to 2.5;
- BzK color-selection (Daddi et al. 2004). The BzK method uses galaxies detected initially in the K-band, with color criteria designed to select galaxies at $1.4 < z < 2.5$, largely independent of their stellar population or dust reddening properties. Late in the VIMOS campaign, we also experimented with applying additional Spitzer/IRAC color criteria to refine the BzK method, but this is largely unimportant for the purposes of the present discussion;
- X-ray sources from the CDF-S and E-CDF-S X-ray catalogs (Giacconi et al. 2002; Lehmer et al. 2005).

No low redshift galaxies were intentionally targeted for the LR-Blue masks, although as we will see in Sect. 6, some foreground interlopers do "contaminate" the color-selected samples, particularly the sub-U-dropouts. A magnitude cut at $B < 24.5$ mag was applied to all target catalogs listed above.

The wavelength range of the VIMOS MR grism is 4000−10 000 Å, similarly to that of FORS2. However, the fringing at red wavelength ($\lambda \geq 7000$ Å) is somewhat stronger than in FORS2, and the VIMOS red throughput is lower. Hence, optical rest-frame spectral features for galaxies at $z > 1$, and the ultraviolet rest-frame spectral features of Lyman break galaxies (LBGs) at $z \gtrsim 4.8$,which would appear at very red optical wavelengths, are harder to detect with VIMOS than with FORS2. Therefore, our VIMOS target selection was limited to brighter galaxies (mainly expected to be at $z < 1.2$), and to color-selected LBGs in the redshift range $2.8 < z < 4.8$. As for the LR-Blue campaign, target selection used the available imaging data and photometry catalogs according to the following criteria:

1. galaxies with $R < 24.5$, with no other color pre-selection, excluding VIMOS LR-Blue targets and objects already observed in other spectroscopic programs. In the later VIMOS campaigns, some preference was given to galaxies detected at 24 μm from the GOODS Spitzer MIPS data (Dickinson et al. in preparation; Chary et al. in preparation), meeting the same $R < 24.5$ mag limit. We do not consider the MIPS-detected sources as a separate category for the purposes of this paper;
2. relatively bright Lyman break galaxies at $i_{775} < 25$, selected as B_{435}, V_{606} dropouts (nominally, redshifts $z \approx 4$ and 5, respectively), according to the same color criteria described in Vanzella et al. (2005, 2006, 2008).

We did not use photometric redshifts, nor did we apply surface brightness selection when selecting galaxies for observations. When designing the masks, we avoided (as much as possible) observing targets that had already been observed in other redshift surveys of the GOODS-S and CDFS region, namely, the K20 survey of Cimatti (2002), the spectroscopic survey of X-ray sources by Szokoly et al. (2004), the VIMOS VLT Deep Survey (Le Fevre et al. 2005) and the ESO/GOODS FORS2 survey (Vanzella et al. 2005, 2006).

3. Observations and data reduction

The VLT/VIMOS spectroscopic observations were carried out in service mode during ESO observing periods P74-P78.

3.1. Preparation of VIMOS observations

For each pointing a short V-band image was taken with VIMOS in advance of the spectroscopic observations. We used this pre-imaging, together with the GOODS WFI R band image, to derive the transformation matrix from the (α, δ) celestial reference frame of the target catalogs to the ($X_{\rm CCD}$, $Y_{\rm CCD}$) VIMOS instrumental coordinate system. This procedure was carried out using the routines *geomap* and *geoxytran* in the IRAF environment. The rms of the residuals from these transformations were ∼0.05 arcsec, ten times better than the accuracy of the matching procedure implemented in the VIMOS mask preparation software (VMMPS, Bottini et al. 2005). This is due to the choice of a higher order polynomial of the fitting procedure, which is not allowed in VMMPS.

Once the target catalog was expressed in the ($X_{\rm CCD}$,$Y_{\rm CCD}$) VIMOS instrumental coordinate system, the next steps in the slit mask design were conducted with the VMMPS tool. After placing two reference apertures on bright stars for each pointing quadrant, slits were assigned to sources drawn from the target catalog. The automated SPOC (Slit Positioning Optimization Code, Bottini et al. 2005) algorithm was run to maximize the number of slits assigned, given the geometrical and optical constraints of the VIMOS set-up. We designed masks with slit widths of one arcsec, and required that a minimum of 1.8 arcsec of sky is left on each side of a targeted object to allow for accurate sky background fitting and removal during later spectroscopic data processing. The spectral range of the VIMOS LR-Blue masks, projected onto the VIMOS CCDs, is short enough that it is possible to have several "layers" of slits whose spectra do not overlap in the dispersion axis. Because of this spectral multiplexing, each GOODS LR-Blue mask could include up to 360 slits in the combined four quadrants. Masks for the VIMOS MR grism were designed with no multiplexing in the dispersion axis to avoid the superposition of zero and negative orders. The combined four quadrants of a GOODS MR mask contained 150 slits on average. The observations were dithered to move targets along the axis of the slits in order to improve the sky subtraction and the removal of CCD cosmetic defects. In the LR-Blue survey, the dithering pattern consisted of three position separated by a step of 1.4 arcsec. In the MR survey, the dithering pattern consisted of five position separated by a step of 1.5 arcsec, in order to provide enough independent pointings to construct and apply a correction for fringing at red wavelengths (see Sect. 3.2).

In the LR-Blue campaign, we used the LR-Blue grism together with the OS-Blue cutoff filter, which limits the bandpass and order overlap. With 1 arcsec slits, the spectral resolution is ∼28 Å and the dispersion is 5.7 Å/pixel. 10 exposures of 24 min each were taken for a total exposure time of 4 h per mask. In the MR campaign, the MR grism was used together with the GG475 filter. With 1 arcsec slits, the resolution is ∼13 Å and the dispersion is 2.55 Å/pixel. 12 exposures of 20 min each were taken for a total exposure time of 4 h per mask. We requested nightly arc-lamp calibrations to measure the wavelength solution of the spectra and reduce problems due to instrument flexure.

3.2. Data reduction

The pipeline processing of the VIMOS-GOODS data is carried out using the VIMOS Interactive Pipeline Graphical Interface (VIPGI, see Scodeggio et al. 2005, for a full description). The data reduction is performed in several interactive steps: locating the spectra in the individual spectroscopic frames, wavelength calibration, sky subtraction and fringing correction, combination of the 2D spectra of dithered observations, extraction of the 1D spectra, and flux calibration. The location of the slits is known from the mask design process, hence, knowing the grism zero deviation wavelength and the dispersion curve, the approximate location of each spectrum on the detectors is known a priori. However, small shifts from the predicted positions are possible. From the predicted position, the location of the spectra are identified accurately on the 4 detectors and an extraction window is defined for each slit. The wavelength calibration is secured by the observation of nightly arc-lamps through each slit mask. Wavelength calibration spectra are extracted at the same location as the object spectra and calibration lines are identified to derive the pixel to wavelength mapping for each slit. The

wavelength to detector pixel transformation is fit using a third order polynomial, resulting in a median rms residual of ~0.7 Å across the wavelength range in the LR-Blue masks and ~0.36 Å in the MR masks. A low order polynomial (second order) is fit along the slit, modeling the sky background contribution at each wavelength position, and subtracted from the 2D spectrum. For the LR-Blue data, fringing is not present, and all 10 exposures of a sequence are directly combined by shifting the 2D spectra following the offset pattern to register the object at the same position. The individual frames are combined with a median, sigma-clipping algorithm to produce the final summed, sky subtracted 2D spectrum. In the case of the Medium Resolution spectra, the fringing is significant at $\lambda > 7000$ Å and needs to be removed. Therefore, a fringing correction is applied before combining the dithered exposures. As the object is moved to different positions along the slit following the dithering pattern, the median of the 2D sky subtracted spectra produces a frame from which the object is eliminated, but that includes all residuals not corrected by sky subtraction, in particular the fringing pattern varying with position across the slit and wavelength. This sky/fringing residual image is then subtracted from each individual 2D sky subtracted frame. The fringing corrected frames are then shifted and combined as in the case of the LR-Blue spectra.

The last step done automatically by VIPGI is to extract a 1D spectrum from the summed 2D spectrum, using an optimal extraction following the slit profile measured in each slit (Horne 1986). The 1D spectrum is flux calibrated using a transformation computed from observations of spectrophotometric standard stars.

Final, we checked each 1D calibrated spectra individually, and removed the most discrepant features manually, cleaning each spectrum of zero order contamination, strong sky lines residuals and negative unphysical features.

3.3. The VIMOS LR-Blue wiggles

Spurious wiggles with amplitude of about 3 to 8% are found in VIMOS MOS spectra taken with the combination of LR_Blue grism and OS_Blue Order Sorting (OS) filter. The position of the wiggles in the spectrum compares well with the wiggles in the response curve of the OS_Blue filter (see also the ESO VIMOS User Manual, Fig. A.3). This clearly indicates that the wiggles originate in the OS filter. The effect of the wiggles should therefore be multiplicative. In principle, spectroscopic screen flat-fields, even taken during the day, would be sufficient to correct the wiggles. However, several aspects make this correction very difficult. The position and amplitude of the wiggles are found to depend on the spectral resolution, which in turn depends on slit width and object size. The wiggle pattern and the overall shape of the flat field spectra depend significantly on the position of the slit in the field of view. In addition, the normalization of flat field spectra is made problematic by the possible overlap of 0th-order spectra from neighboring slits. For these reasons we prefer not to correct the wiggles observed in the LR-Blue spectra.

3.4. Target coordinates

The rotation angle of the VIMOS GOODS pointings (−20 deg) is different from the default values accepted by VIPGI (0 and 90 deg). Therefore, VIPGI does not provide the astrometry of the extracted spectra. The only information provided by VIPGI are the coordinates in mm on the focal plane stored in the VIPGI *object table*. To overcome this problem, we transform the

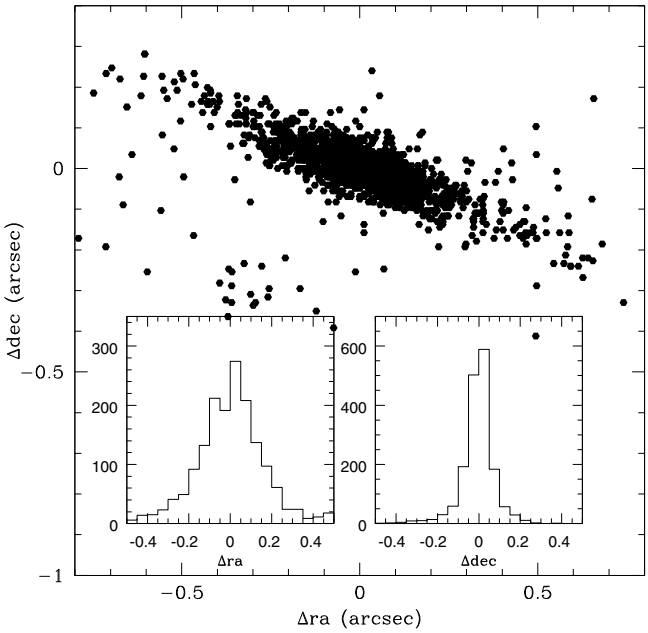

Fig. 2. Δra and Δdec residual distribution of the cross-correlation between "reconstructed" WFI coordinates and original target coordinates. The strong distortion of VIMOS quadrants is not completely removed, as indicated by the trend in the Δra-Δdec distribution shown in the main panel. However, the rms of the residuals is smaller than 0.2 arcsec in both axes, as shown by the histograms in the inset panels, ensuring accurate target identification.

focal plane coordinates of each object into CCD coordinates using the appropriate distortion solution recorded in the headers of our VIMOS observations. Slits which contain only one object (only one spectrum extracted) are used to calculate the transformation matrix from VIMOS coordinates to the GOODS *R*-band WFI CCD coordinates through the IRAF routines *geomap* and *geoxytran*. Finally, the WFI $X_{\rm CCD}$ and $Y_{\rm CCD}$ assigned to each extracted spectrum are converted to α, δ on the basis of the GOODS WFI *R*-band astrometry. These "reconstructed" coordinates are, then, matched to the original GOODS VIMOS target catalog to identify the primary targets as well as any serendipitous objects extracted from our slits. For objects that match, we assign the original coordinates of the target GOODS catalog. Otherwise the "reconstructed" coordinates are used. The coordinate conversion is done separately quadrant by quadrant. Figure 2 shows the distribution of the Δra and Δdec in the cross-correlation of the reconstructed WFI coordinates and the original targets coordinates. The very strong distortion of the VIMOS CCD is not completely removed, as indicated by the trend in the Δra-Δdec distribution shown in the main panel. This is due to the fact the we can use few objects to calculate the transformation matrix from VIMOS to the GOODS *R*-band WFI CCD coordinates. However, the rms of the cross-correlation is smaller than 0.2 arcsec in both coordinates, allowing for reliable identification of the targets from the imaging catalogs.

It is worth noting that, due to a bug, VIPGI assigns incorrect focal plane coordinates to a small number of objects in slits from which more than two spectra were extracted. In the released catalog the slit center coordinates are assigned to these objects, with an uncertainty of ±5 arcsec. These objects are, then, normally processed in the data reduction procedure. We find 82 cases of this from the LR-Blue campaign, of which 80% have no redshift determination, and 34 in the MR campaign, of which 50% have no redshift determination. The failures to measure redshifts

are simply due to the low S/N in these spectra. Those objects are given focal plane coordinates $x_{\rm fp} = 0.0, y_{\rm fp} = 0$. Moreover, on the basis of the reconstructed WFI coordinates, these objects would be located completely out of the slits where they should be. The complete list of those objects is available at http://archive.eso.org/cms/eso-data/data-packages.

4. Redshift determination

2344 spectra have been extracted from the 6 LR-Blue masks and 968 have been extracted from 6 MR masks. From these, we have been able to determine 1481 redshifts in the LR-Blue campaign and 656 in the MR campaign. 33% of the LR-Blue slits and 18% of the MR slits contain more than one spectrum. Most of the secondary spectra obtained provide additional observations of known targets. We have identified 2235 unique LR-Blue objects and 886 unique MR objects.

Redshift estimation has been performed by cross-correlating the individual observed spectra with templates of different spectral types. Templates for ordinary S0, Sa, Sb, Sc, and elliptical galaxies were used to measure redshifts of relatively low redshift galaxies. At higher redshifts, where the VIMOS observations mainly sample the ultraviolet rest frame, several different spectral templates for Lyman break galaxies, BzK-selected galaxies, and AGN were used. The cross-correlation is carried out using the *rvsao* package (*xcsao* routine, Kurtz & Ming 1998) in the IRAF environment. In particular, a trial-and-error approach is used for the $z > 1.8$ galaxies, whose redshift determination is made difficult by the low S/N ratio of the spectral absorption features and the wiggles in the LR-Blue spectrum.

In the large majority of the cases the redshift has been determined through the identification of prominent features of galaxy spectra:

- at low redshift the absorption features: the 4000 Å break, Ca H and K, Hδ and Hβ in absorption, g-band, MgII 2798;
- and the emission features: [O II]3727, [O III]4959,5007, Hβ, Hα;
- at high redshift: Lyα, in emission and absorption, ultraviolet absorption features such as [Si II]1260, [O I]1302, [C II]1335, [Si IV]1393,1402, [S II]1526, [C IV]1548,1550, [Fe II]1608 and [Al III]1670 (see also Fig. B.1 of the appendix).

In analogy to the complementary GOODS-FORS2 redshift campaign (Vanzella et al. 2005, 2006, 2008), we use four flag values to indicate the quality of each redshift estimate. The determination of the quality flag is done in two steps. As a first step, the assignment of the quality flag is done during the cross-correlation of the spectrum with the templates on the basis of the cross-correlation coefficient provided by the routine *xcsao* in the IRAF environment. The quality flags are assigned according to the following criteria (see also the appendix for several examples):

- flag A: high quality, values of the *xcsao* correlation coefficient $R \geq 5$; emission lines and strong absorption features are well identified;
- flag B: intermediate quality, values of the *xcsao* correlation coefficient $3 \leq R < 5$; one emission line plus few absorption features are well identified;
- flag C: low quality, values of the *xcsao* correlation coefficient $R < 3$, features of the continuum not well identified.
- flag X: no redshift estimated, no features identified.

As a second step, each spectrum, with superposed labels indicating the main spectral features, is checked by eye by several different people, who refine the redshift determination and the quality flag assignment. A good agreement of the different redshift estimates has been found for nearly all of the flag A spectra, ~80% of original quality B cases, and ~60% of original C cases. In case of disagreement the object is assigned a lower quality flag. On average, each spectrum is checked more then three times.

In ~15% of the cases the redshift is based only on one emission line, usually identified with [O II]3727 or Lyα. In these cases, the continuum shape, the presence of breaks, the absence of other spectral features in the observed spectral range, and the broad band photometry are considered in the redshift evaluation. In general these solo-emission line redshifts are classified as "likely" (B) or "tentative" (C) if no other information is provided by the continuum. In a few cases, the quality flag is set to A if the photometry or the availability of photometric redshifts help in distinguishing between high and low redshift sources (see Kirby et al. 2007, for the DEEP2 survey).

The internal redshift accuracy can be estimated from a sample of galaxies which have been observed twice in independent VIMOS mask sets. We find 39 such cases in the LR-Blue masks and 40 in the MR masks, with quality flag A or B. ~45% of these objects have been observed as serendipitous targets. The distribution of measured redshift differences is presented in Fig. 3. The mean of the Δz distributions is close to zero ($\sim 10^{-5}$) for both the LR-Blue and MR observations. The redshift dispersion is $\sigma_z = 0.0013$ (~400 km s^{-1}) for the LR-Blue objects and $\sigma_z = 0.0007$ (~200 km s^{-1}) for the MR redshifts. This latter estimation is in very good agreement with the value obtained in the GOODS-FORS2 survey (Vanzella et al. 2005), conducted on similar objects using similar spectral resolution and spectral range as VIMOS MR. We note that the mean values of the redshift estimation uncertainty estimated in this way are ~3 times larger than the mean error ($\sigma_z = 0.0004$ in the LR-Blue survey and $\sigma_z = 0.0002$ in the MR survey) calculated by the IRAF routine *xcsao*.

4.1. The success rate

4.1.1. The VIMOS LR-Blue targets

We measured redshifts for 70% (63% including also the secondary serendipitous objects) of the observed LR_Blue spectra. However, to estimate the success rate of the surveys we use only the objects with high quality flags, A and B. In the LR-Blue survey the success rate is 48% for the original target sample and 39% if we consider also the secondary targets. The serendipitous sources, which account for 33% of the sample, are usually faint neighbors and lie often at the edge of the 2D spectrum. Moreover, they are not subject to the color pre-selection used for the primary LR-Blue targets, and it is likely that they often lie at redshifts which are not accessible to the wavelength range covered by the VIMOS LR-Blue grism (see Sect. 5.1 for details). For these objects the success rate is very low, ~20%. We have investigated how the success rate depends on the target selection and on the redshift windows. Figure 4 shows the color-magnitude diagram of different targets and for different redshift quality. In particular, the first and central panels show the $B - R$ vs. B diagram of the LR-Blue targets in case of successful redshift determination (top panel) and in case of failure (C or X cases). The latter cases lie all at very faint B magnitudes, indicating that the failures are mainly due to the poor S/N of the spectra. As described in Sect. 2.2, the LR-Blue targets can be divided in 4 families: U-dropouts, BzK objects, sub-U-dropouts

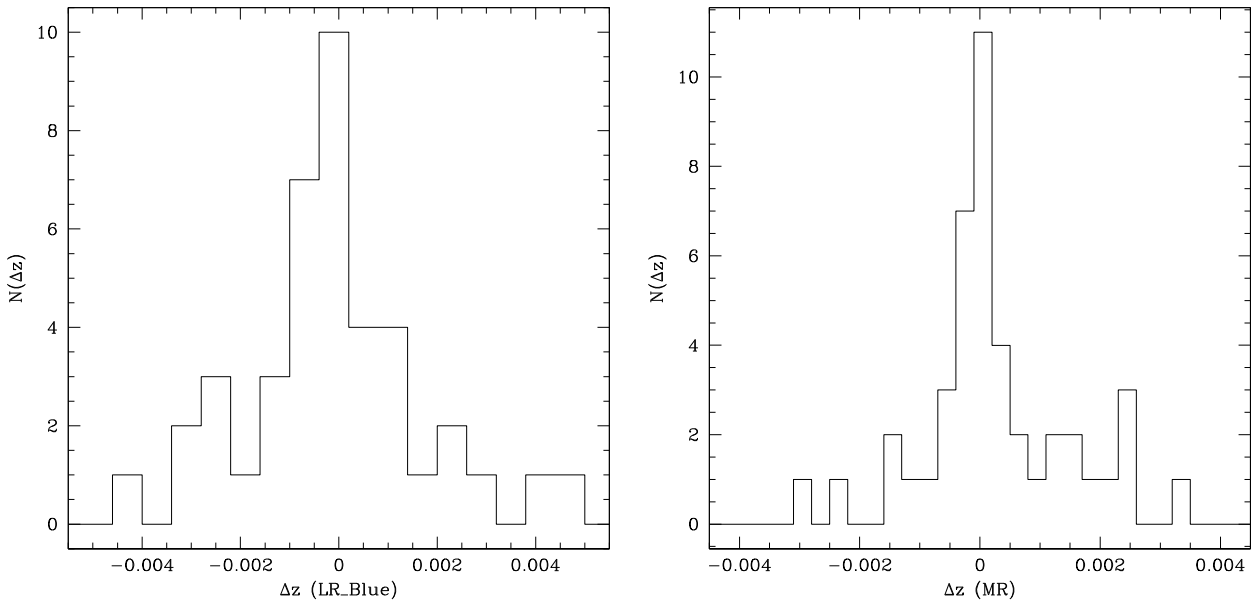

Fig. 3. Redshift differences between objects observed twice or more in independent VIMOS LR-Blue (*left panel*) and MR (*right panel*) observations. The distribution has a dispersion of $\sigma_z = 0.0013$ in the LR-Blue campaign and $\sigma_z = 0.0007$ in the MR campaign.

and X-ray sources. The BzK and sub-U-dropouts samples have considerable overlap. In this discussion, we consider these two families separately. Table 1 shows the fraction of targets observed in the analyzed masks and the corresponding success rate for each target family. The BzK objects have the lowest success rate. 64% of those objects have flag C or no redshift (flag X). All of the other target families have a success rate of ~50%. In addition we find a strong dependence of the success rate on the redshift window. In particular:

- objects at low redshift ($z_{\rm spec} < 1$) and in the range $2.2 \leq z_{\rm spec} \leq 3.5$ have the highest fraction of A flags, ~60%;
- very high redshift galaxies ($z_{\rm spec} > 3.5$) have mainly quality flag B because the Lyα in emission is in the very red part of the spectrum, and other features are not well identified;
- objects at $1.8 < z_{\rm spec} < 2.2$ show the highest fraction of insecure redshift determinations (percentage of the C flag determination ~65%).

There are two main reasons for the high failure rate at redshift $1.8 < z_{\rm spec} < 2.2$ and for the BzK galaxies, many of which are expected to lie in this redshift range. The first is that the Lyα is often outside the spectral range covered by the LR-Blue grism, at $\lambda < 3600$ Å. Therefore, other "secondary" spectral features, such as SII, OI, CII, SiIV, SII, and CIV, have to be used to estimate the redshift. However, these features are not as strong as Lyα in absorption or emission. In addition, at $\lambda < 4000$ Å the VIMOS efficiency drops very quickly and the presence of the wiggles described in Sect. 3.3 makes the redshift determination very insecure. In fact, only the very bright sources have S/N ratios at $\lambda < 4000$–4200 Å high enough to identify the "secondary" features of the continuum.

4.1.2. The MR targets

We measured redshifts for 75% (67% including also the secondary serendipitous objects) of the observed MR spectra. In the VIMOS MR campaign the overall success rate (A+B flag redshifts) is 60% and reaches the 65% level if only the primary targets are considered. We do not note any dependence on the target selection criteria or redshift windows. The bottom panel of Fig. 4 shows the $i-z$ vs. z diagram for the MR primary targets. The black dots are the high quality (A and B flag) MR redshifts at $z < 0.8$, the empty circles are (A and B flag) MR redshifts at $z > 0.8$. The stars represent the C and X cases. The C and X cases are concentrated in the region populated by objects at $z > 0.8$. This is due to the fact that above this redshift the main spectral features enter the wavelength range where both the OH sky emission lines and the CCD fringing are strong, at $\lambda > 7500$ Å, making line identification very difficult.

5. Discussion

5.1. Reliability of the redshifts – comparison with previous surveys

A practical way to assess the reliability of the redshifts is to compare the present results with independent measurements from other surveys. For this purpose we use the results of four other surveys conducted on the same field: the GOODS-FORS2 campaign (Vanzella et al. 2005, 2006, 2008), which mainly targeted faint galaxies whose red $i-z$ colors imply redshifts $z > 1$, as well as $z > 3.5$ Lyman break galaxies; the K20 survey of K-band selected galaxies (Cimatti et al. 2002); the Szokoly et al. (2004) survey of (mainly) CDFS X-ray sources; and the VVDS survey (Le Fevre et al. 2005), which was limited by I-band apparent magnitude and the IMAGES survey (Ravikumar et al. 2007) limited to $M_J < -20.3$. To create a secure redshift reference sample, we have selected only the high quality redshift determinations of those surveys: GOODS FORS2 quality A and B, K20 quality 1, VVDS quality 3 and 4 and Szokoly et al. 2004 quality 3 and 2+ redshifts, which all nominally have a confidence level higher than 95%.

Among the LR-Blue redshift determinations, there are 113 VIMOS objects in common with this high quality reference sample within an angular matching tolerance of 0.5 arcsec. 58 of them have VIMOS quality flag A, 16 have flag B, 16 have flag C and 23 do not have a redshift estimation (flag X). These 23 quality X objects have redshifts in the other surveys that fall in the redshift range $0.8 < z < 1.7$, which is not readily accessible to

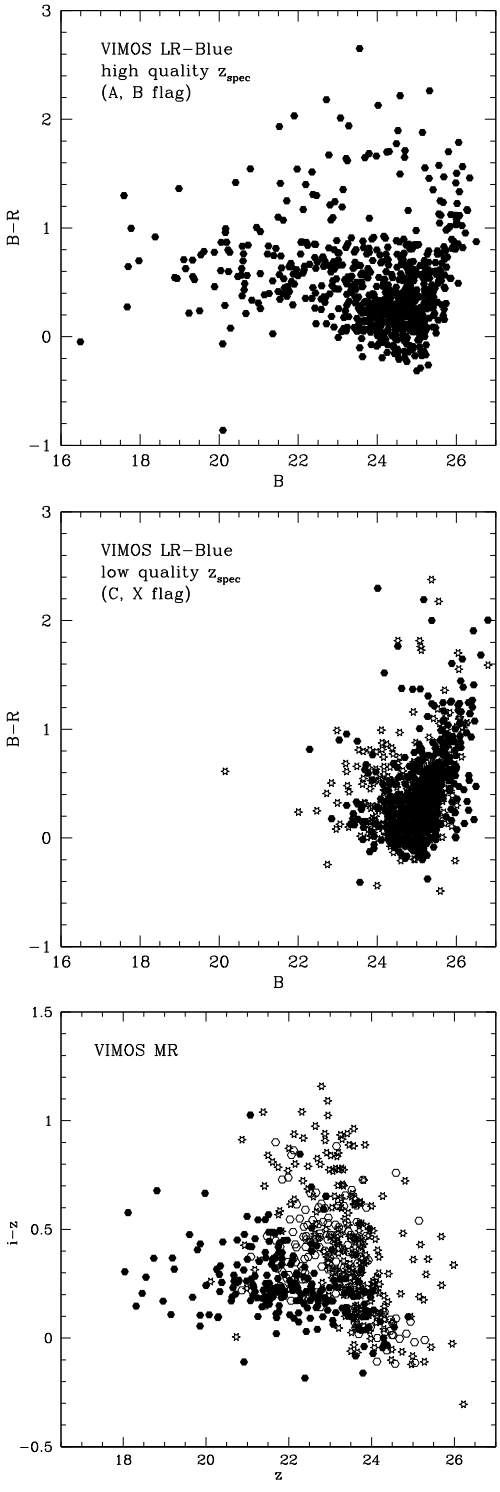

Fig. 4. Color−magnitude diagram of the LR-Blue and MR primary targets. The first panel shows the $B - R$ vs. B diagram for A and B high quality LR-Blue redshifts. Low quality LR-Blue redshifts (C flag, dots) and failure (X flag, stars) are shown in the central panel. The bottom panel shows the $i - z$ vs. z diagram for the MR primary targets. The black dots are the high quality (A and B flag) MR redshifts at $z < 0.8$, the empty circles are high quality (A and B flag) MR redshifts at $z > 0.8$. The stars represent the C and X cases.

the VIMOS LR_Blue observations given their wavelength coverage. 27 cases of the A, B and C quality redshifts show "catastrophic" discrepancies ($|z_{\rm VIMOS} - z_{\rm FORS2/K20/CDF/VVDS}| > 0.015$).

Table 1. Success rate of the GOODS VIMOS LR-Blue campaign. The first column lists the name of the target family, the second column lists the fraction of the target catalog due to the corresponding color selection (BzK and sub-dropout family overlap largely but they are considered as separated family in the table). The third column lists the success rate (fraction A+B flag objects) of each target family. The last four columns list the percentage of A, B, C and X flag redshift determinations, respectively.

Target	Fraction	s.r.	A	B	C	X
U-dropouts	16%	49%	35%	14%	15%	36%
BzK	51%	36%	24%	12%	21%	43%
sub-U-dropouts	66%	51%	35%	16%	16%	33%
X-ray	5%	51%	37%	14%	14%	35%

These account for 5 of the VIMOS flag A objects, 8 of the flag B sources, and 11 of the flag C sources.

After visual comparison of the VIMOS and FORS2/K20/CDF/VVDS spectra we find that 3 of the 5 VIMOS quality A spectra with "catastrophic" discrepancies are likely to be incorrect GOODS/VIMOS redshift determinations:

- VIMOS GOODS_LRb_001_q2_1_1 versus FORS2 GDS_J033217.78-274823.8 (flag A): the [OIII] in emission is identified in the FORS2 spectrum and it is hidden by a strong sky line residual in the VIMOS spectrum. Thus, the [OII] in the VIMOS spectrum is misclassified as Lyα due to the absence of H_β and [OIII] emissions.
- VIMOS GOODS_LRb_001_1_q1_51_1 versus FORS2 GDS_J033226.67-274013.4 (flag A): the [OII] in the FORS2 spectrum is identified at $z = 1.612$, a redshift window not accessible to VIMOS LR-Blue. No emission lines are visible in the VIMOS spectrum and the low S/N UV absorption features are misclassified.
- VIMOS GOODS_LRb_001_q2_35_1 versus VVDS VVDS 32126 (flag 3, observed with the VIMOS LR-Red grism): the strong UV absorption features identified in our VIMOS LR-Blue spectrum provide a *xcsao* correlation coefficient similar to that of the FeII and NeV absorption features identified in the VVDS LR-Red spectrum. We have combined the two spectra and re-performed the cross correlation. The highest correlation peak corresponds to the VVDS redshift value
- VIMOS GOODS_LRb_001_q3_71_2 versus VIMOS LR-Red VVDS 16975 (flag 24): the VIMOS LR-Blue source is an emission line galaxy and the reference VVDS spectrum is clearly an early type galaxy without any emission line. The two spectra can not refer to the same object. Since 16975 is a secondary object and not a primary target, we suspect that the coordinates provided by VIPGI (used to reduce the VVDS data) could be wrong as explained in Sect. 3.4. Thus, we consider our VIMOS redshift estimation correct, although the object identification may be incorrect.
- VIMOS GOODS_LRb_002_q2_55_1 versus FORS2 GDS_J033221.94-274338.8 (flag A): the strong emission line in the VIMOS spectrum is identified as a Lyα due to the absence of H_β and [OIII] emission and due to the photometry (the target was selected to be a U-dropout). The emission line could be classified as a [OII] at much lower redshift ($z = 0.166$) with a much lower *xcsao* correlation coefficient. In either case, the FORS2 redshift is not in agreement. We have combined the two spectra and re-measured the redshift. The correlation gives a good result only with a Lyα emitter template at $z = 2.576$. No match is found for the emission seen in the FORS2 spectrum, which has a very low S/N. We

think that the line identified as [OII] in the FORS2 spectrum is instead due to a fringing residual since it is sitting on a sky line. Thus, we believe that the VIMOS redshift estimation is likely to be correct.

The resulting confidence level for the flag A redshift determinations is 95% (3 mistakes out of 58 redshift determinations). Among the flag B spectra showing "catastrophic" discrepancies, 6 VIMOS redshift determinations are wrong, mainly due to the presence of sky residuals and 0th order contamination from neighboring spectra, and only 2 are more convincing than the FORS2/K20/CDF/VVDS determinations. The resulting confidence level is 62% (6 mistakes out of 16 redshift determinations). For all of the Flag C discrepancies, the FORS2/K20/CDF/VVDS redshift determinations are more convincing than the ultraviolet features identified in the LR-Blue spectra. The resulting confidence level is 31%. However, it is important to note that in most cases, the VIMOS flag C is assigned to redshifts in the range $1.8 < z < 2.2$, as explained in Sect. 4.1. The surveys considered in this comparison (FORS2, K20, CDF and VVDS) were not optimized (mainly, in terms of wavelength coverage) to measure redshifts in this range. Thus, such comparisons can only reveal the mistakes in the GOODS/VIMOS redshift sample, and cannot provide confirmations to our estimates. In conclusion, 19 redshift determinations out of 90 are wrong, resulting in an overall confidence level of 78% in the LR-Blue VIMOS redshifts. For the 71 cases out of 90 which show good agreement, we find a mean difference $\langle z_{\rm LR-Blue-VIMOS} - z_{\rm FORS2/k20/VVDS}\rangle = 0.0018 \pm 0.0019$, which confirms the mean uncertainty Δz found in Sect. 4.

The comparison between the VIMOS MR redshift determinations and FORS2/K20/CDF/VVDS measurements is simplified by the fact that our MR observations cover a similar wavelength range to those observed in the other surveys. There are 94 VIMOS objects in common with the high quality reference sample within a positional tolerance of 0.5 arcsec. 69 of them have VIMOS quality flag A, 17 have quality flag B and 8 have quality flag C. We find 5 "catastrophic" discrepancies: 1 has flag A, 1 has flag B and 3 have flag C:

– flag A case GOODS_MR_new_1_d_q3_22_1 versus FORS2 GDS_J033243.19-275034.9 (flag A): an accurate analysis is provided by Vanzella et al. (2006, see their Fig. 2). The continuum shows increasing bumps/bands in the red, very similar to typical cold stars. After visual inspection of the ACS color image Vanzella et al. (2006) concluded that GDS_J033243.19-275034.9 is a simultaneous spectrum of two very close sources: a star and a possible high-z galaxy;
– B flag case VIMOS GOODS_MR_new_1_d_q2_21_2 versus FORS2 GDS_J033249.04-2705015.5 (flag A): the spectral features used to identify the VIMOS redshift are all at $\lambda > 7500$, where the fringing is very strong. The corresponding FORS2 spectra, which suffer less of fringing, show more convincing spectral features.

In the 3 flag C cases, the FORS2/K20/CDF/VVDS redshift estimates seem to be more robust than the VIMOS redshifts. In all three cases the spectral features used to identify the redshift are in the region strongly affected by fringing.

Thus, we obtain a confidence level of 98% for the quality A MR redshifts (1 mistake out of 69 redshifts), 94% for the quality B redshifts (1 mistakes out of 17 determinations) and 62% for the quality C cases (3 mistakes out of 8 determinations). The overall confidence level of the redshift determinations of the MR redshift survey is 95%. For the 89 cases

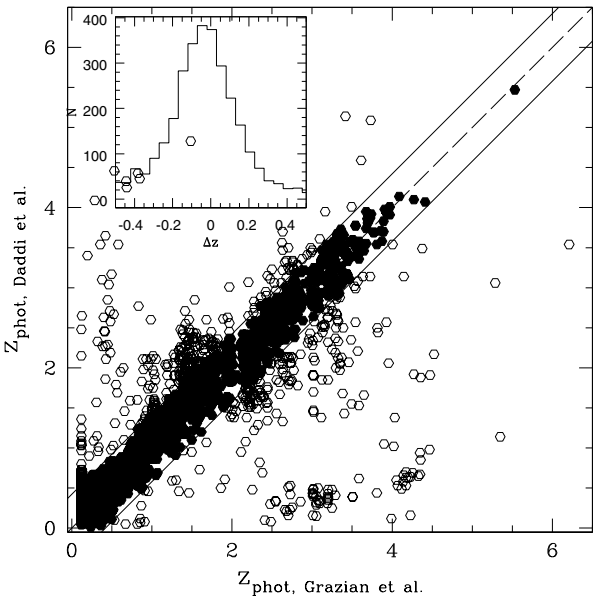

Fig. 5. Comparison of the GOODS-MUSIC and the GOODS photometric redshift catalog. The small inset panel shows the distribution of redshift differences, $\Delta z = z_{\rm MUSIC} - z_{\rm GOODS}$, with $\sigma = 0.13$. The dashed line in the main panel shows the line of photometric redshift quality, and the solid lines indicate the $\pm 3\sigma$ range, $|\Delta z| < 0.39$.

out of 94 which show good agreement, we find a mean difference $\langle z_{\rm MR-VIMOS} - z_{\rm FORS2/k20/VVDS}\rangle = 0.0013 \pm 0.0012$.

5.2. Reliability of the redshifts – comparison with photometric redshift

An alternative way to assess the reliability of the redshifts is to compare the present results with accurate photometric redshifts. Photometric redshift determinations are inevitably plagued by a rather high incidence of catastrophic failures, and can exhibit biases depending on the redshift determination procedure applied. Thus, to partially mitigate these concerns, we simultaneously consider two different photometric redshift catalogs: the GOODS-MUSIC catalog (Grazian et al. 2006) and a GOODS photometric redshift catalog (Daddi et al., private communication). The GOODS-MUSIC photometric redshifts are based on a high quality multiwavelength (from 0.3 to 8.0 μmm) catalog, which includes accurate "PSF-matched" ACS, JHKs ESO VLT, Spitzer IRAC and the first 3 h U-band VLT-VIMOS magnitudes. They were trained on the high quality GOODS-FORS2 and VVDS spectroscopic redshifts. The Daddi et al. (private communication) catalog is based on most of the same GOODS imaging data used by Grazian et al., including IRAC but not the VIMOS U-band, but the two catalogs use independent photometric measurements (different software, apertures, etc.). The Daddi photometric redshifts were trained using high quality spectroscopic redshifts from GOODS-FORS2, K20, and GMASS (Kurk et al., in preparation). For our purposes, we have cross-correlated the two photometric redshift catalogs and created a high quality reference sample which includes only those objects with concordant GOODS-MUSIC and GOODS redshift estimations. We have calculated the standard deviation of the photometric redshift differences, $\Delta z = z_{\rm Grazian} - z_{\rm Daddi}$, finding $\sigma(\Delta z) = 0.13$, We define the photometric redshift reference sample to be those objects with $|\Delta z| < 3\sigma$, i.e., $|\Delta z| < 0.39$. Figure 5 shows the comparison of the Grazian and Daddi photometric redshifts. The filled circles lying within the 3σ lines (the solid lines in the

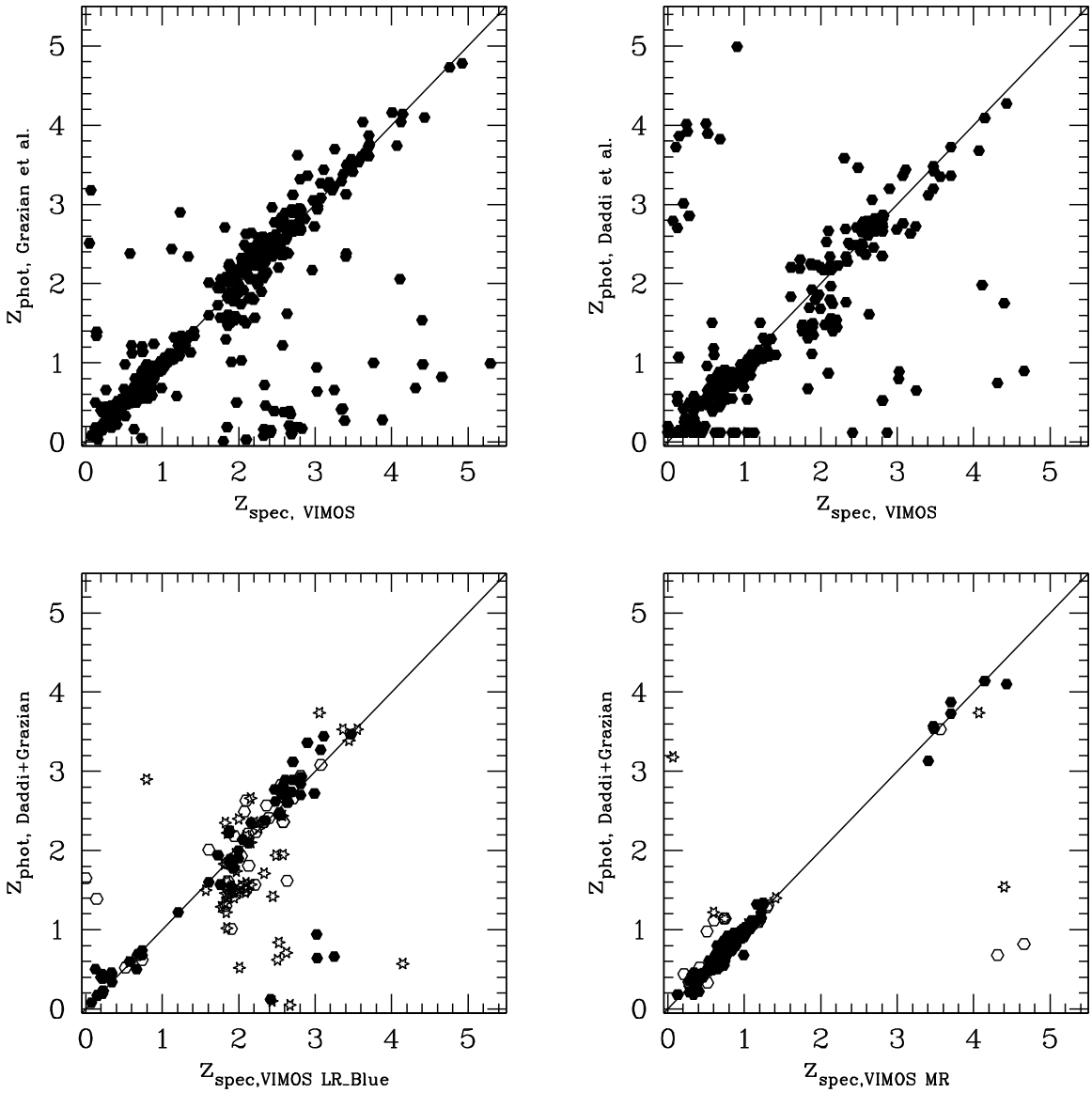

Fig. 6. z_{spec} versus z_{phot}. The *two top panels* show the comparison between the GOODS VIMOS (LR-Blue + MR) high quality z_{spec} and the GOODS-MUSIC z_{phot} of Grazian et al. (2006) (*top left panel*) and the GOODS z_{phot} of Daddi et al. (private communication, *top right panel*). In both cases there is a rather high percentage of discrepancies located in different regions of the diagram. If we compare the LR-Blue (*bottom left panel*) and the MR (*the bottom right panel*) z_{spec} only with z_{phot}, which are consistent within 3σ in the GOODS-MUSIC and GOODS catalogs, the agreement is much higher. In both *bottom panels* the filled circles are flag A z_{spec}, the empty circles are B flag z_{spec} and the stars are C flag z_{spec}.

figure) are those included in our photometric redshift reference sample, and the empty circles are excluded from it.

Next, we have compared this high quality reference z_{phot} sample with our VIMOS LR-Blue and MR spectroscopic redshift measurements. Figure 6 shows the result of the comparison. We define "catastrophic" discrepancies to be those measurements with $|z_{spec} - z_{phot}| > 3\sigma$. For the LR-Blue survey:

- we find 150 common objects between the z_{phot} reference sample and the LR-Blue spectroscopic catalog. 65 of them have flag A, 34 have flag B and 51 have flag C;
- there are 4 flag A "catastrophic" discrepancies: 1 is a secure Lyman break galaxies with strong Lyα in emission and well identified ultraviolet features, and is not consistent with the $z_{phot} = 0.94$. In the remaining 3 spectra the emission line is identified as Lyα but it could be also an [OII] as suggested by the z_{phot}. Thus 3 z_{spec} determinations out of 65 can be considered wrong, which confirms a confidence level of 95% in the low resolution flag A redshifts;
- we find 8 flag B discrepancies: 2 of them are secure low redshift emission line galaxies ([OII], Hβ and [OIII] well identified). The remaining 6 spectra are solo-emission line ([OII] or Lyα) spectra with few other low S/N features identified. If the line is identified differently ([OII] instead of Lyα or vice-versa) the resulting z_{spec} is consistent with z_{phot}. Thus, we consider these measurements wrong. The resulting confidence level is 82%;
- there are 23 flag C z_{spec} which are not confirmed by the z_{phot}, which results in a confidence level about 55%.

We list below the results obtained for the MR survey:

- we find 177 common objects between the z_{phot} reference sample and the MR spectroscopic catalog. 123 of them have flag A, 37 have flag B and 17 have flag C;

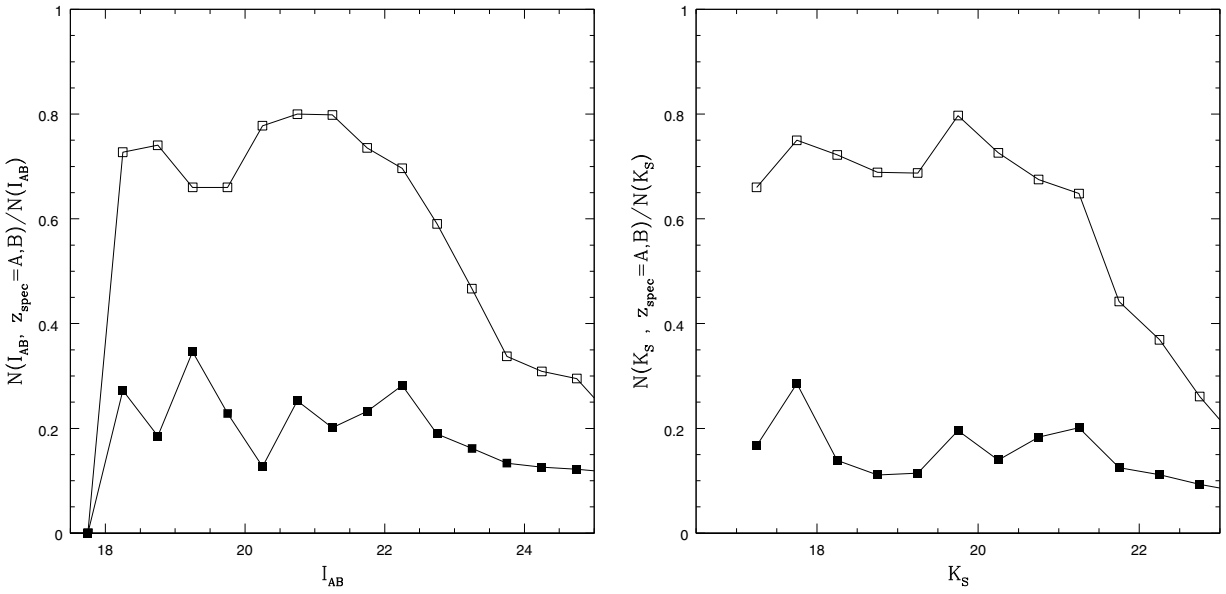

Fig. 7. Completeness level of the VIMOS survey (filled squares) and of the GOODS-S master catalog (empty squares) as a function of the I (*left panel*) and K_S (*right panel*) AB magnitudes.

- there are 2 flag A "catastrophic" discrepancies. Both cases are secure low redshift emission line galaxies ([OII], Hβ and [OIII] well identified). Thus the confidence level of the MR A flag redshifts, in this test, is 100%;
- we find 6 flag B discrepancies: 2 of them are secure low redshift emission line galaxies. In the remaining 4 spectra, the emission line is located in the fringing region and could be misclassified. The resulting confidence level is 89%;
- there are 4 flag C $z_{\rm spec}$ which are not confirmed by the $z_{\rm phot}$, which results in a confidence level of 76%.

5.3. The survey completeness

The following analysis is restricted only to the GOODS-S area, which is the main region of interest of the overall GOODS-VIMOS spectroscopic survey. Therefore, we consider for this analysis only VIMOS LR-Blue and MR spectroscopic sources belonging to the GOODS-S region proper (i.e., the area covered by deep HST/ACS and Spitzer data), and we apply the same restriction to any other spectroscopic catalog used for creating the GOODS-S master catalog (see below for details).

5.3.1. Completeness as a function of magnitude

The main purpose of the two complementary GOODS-South redshift surveys, the FORS2 and VIMOS campaigns, is to provide a highly complete spectroscopic sample down to i_{775} = 25 mag. Thus, it is important to know which is the real level of completeness reached so far after the completion of the whole FORS2 survey and 60% of the VIMOS survey. For this purpose we have created a GOODS-S spectroscopic "master catalog". This is namely the compilation of all high quality spectroscopic redshifts available in the GOODS-S region: GOODS FORS2 quality A and B, VIMOS LR-Blue and MR quality A and B, K20 quality 1, VVDS quality 3 and 4, Szokoly et al. (2004) quality 3 and 2+ and Ravikumar et al. (2007) quality 2 redshifts. We have cleaned the GOODS-S spectroscopic "master catalog" of duplicate observations. In case of double or multiple observations we made a visual inspection of the different spectra and chose the most convincing redshift estimate. Figure 7 shows the completeness level of the VIMOS survey (filled squares) and of the GOODS-S "master catalog" (empty squares) as a function of the I (left panel) and K_S (right panel) AB magnitudes. The final completeness level achieved in the field by the GOODS-S spectroscopic "master catalog" (empty squares in the figure) is on average ∼70% down to i_{AB} = 22.5 mag and K_s = 21.5 mag, respectively. At fainter magnitudes the completeness level decreases to ∼20%.

5.3.2. Completeness in different redshift bins

In principle, the selection function of a spectroscopic survey could be estimated by comparison with appropriate simulations able to reproduce the results of the applied target selection criteria. In the case of the FORS2 and VIMOS campaigns this is complicated by the fact that the selection criteria are not uniform throughout the survey. In fact, they were tailored for each observing run in order to optimizing the survey success rate in terms of redshift estimation on the basis of partial results from previous observations. To overcome this problem we use a different approach, comparing our spectroscopic redshift catalog with a fairly complete photometric redshift catalog. As in the previous section we use two $z_{\rm phot}$ catalogs, the GOODS-MUSIC catalog of Grazian et al. (2006) and the GOODS catalog of Daddi et al. (2007b), to control possible biases. The largest fraction of the GOODS-MUSIC sample is 90% complete at $z \sim 26$ and $Ks \sim 23.8$ mag (AB scale). In a similar way, the GOODS catalog of Daddi et al. (2007b) includes all the GOODS sources with $Ks < 23.8$ mag. Since we are calculating the selection function of our spectroscopic catalog in the ACS i band, we have checked that both $z_{\rm phot}$ catalogs are able to reproduce the observed i-band number counts band down to the required magnitude limit (i_{775} = 25). As shown in the left panel of Fig. 8, both $z_{\rm phot}$ catalogs are able to reproduce the same coarse-grain redshift distribution within 3σ (considering only Poisson errors). The redshift bin is chosen to be $\delta z = 0.3$, similar to the 3σ uncertainty obtained in the comparison of the two $z_{\rm phot}$ catalogs. The same panel shows also the coarse-grain redshift distribution of the VIMOS (LR-Blue+MR, the filled circles) survey and

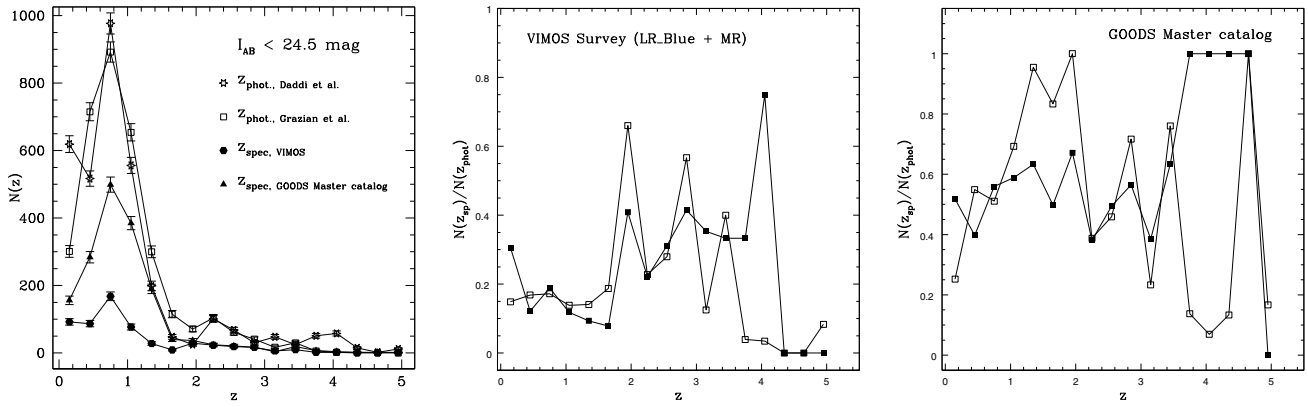

Fig. 8. Completeness level of GOODS spectroscopy in the CDF-S in several redshift bins. The left panel shows the coarse-grain redshift distribution of the $z_{\rm phot}$ catalogs considered for the comparison and the spectroscopic catalogs (GOODS VIMOS catalog and the GOODS master catalog containing all the available spectroscopic redshifts in the CDF-S). The central and the right panels show the spectroscopic completeness level of the GOODS VIMOS and the master catalogs, respectively, in several redshift bins. The completeness level is defined as the ratio $N(z_{\rm spec})/N(z_{\rm phot})$ in each redshift bin. In both panels the empty squares show the $N(z_{\rm spec})/N(z_{\rm phot})$ obtained from the GOODS-MUSIC catalog of Grazian et al. (2006) and the filled squares show the $N(z_{\rm spec})/N(z_{\rm phot})$ obtained from the GOODS catalog of Daddi et al. (private communication).

of the GOODS-S "master catalog". The completeness level in each redshift bin is calculated as the ratio $N(z_{\rm spec})/N(z_{\rm phot})$. The central panel of Fig. 8 shows the redshift-dependent completeness level of the whole GOODS-VIMOS survey. The GOODS-VIMOS survey samples a small fraction (∼10%) of the total galaxy population at $i_{AB} < 25$ mag a $z < 1.5$. This is expected because the LR-Blue targets, which account for 2/3 of the whole GOODS-VIMOS spectroscopic sample, are selected to be at $z > 2$. Indeed, at $2 < z < 3.5$ the GOODS-VIMOS survey samples ∼40% of the whole high redshift population at $i_{AB} < 25$ mag. We adopt the same approach also for analyzing the "selection function" of the GOODS-S spectroscopic "master catalog". The right panel shows the redshift-dependent completeness level in this case. The completeness level of the GOODS master catalog is ∼60% up to $z \sim 3.5$. This is reinforced by the fact that the two $z_{\rm phot}$ catalogs provide consistent results within the error bars up to this redshift. At higher redshift, the results obtained with the two different $z_{\rm phot}$ catalogs are too discrepant (more than 3σ; the error bars are not shown in the central and right panels for clarity). This large discrepancy does not allow us to draw any conclusion in this redshift range. It is worth noting that high level of completeness in the $2 < z < 3.5$ redshift bins is mainly due to the GOODS-S VIMOS spectroscopic survey, which accounts for almost 65% of the whole spectroscopic redshifts available in the GOODS-S region in that redshift range.

5.4. Redshift distribution and large scale structure

Figure 9 shows the fine-grain redshift distribution of the VIMOS LR-Blue (top panel), the VIMOS MR (the central panel) and the GOODS master spectroscopic catalog (the bottom panel). The smaller panels within each main panel show redshift regions of particular interest. Only the very high quality redshifts have been used for the analysis (flag A and B VIMOS and FORS2 redshift, flag 1 K20, flag 3 and 4 VVDS redshifts and flag 2 and 3 of Szokoly et al. 2004; flag 2 Ravikumar et al. 2007). To assess the significance of the observed large scale structures we follow a procedure suggested by Gilli et al. (2003) and similar to the one of Cohen et al. (1999). The sources are distributed in $V = c\ln(1+z)$ rather then in redshift, since dV corresponds to local velocity variations relative to the Hubble expansion. The observed distribution is then smoothed with a Gaussian with $\sigma_S = 300\ {\rm km\,s^{-1}}$ (see Fig. 10) to obtain the "signal" distribution. Since there is no a priori knowledge of the "background" distribution, we heavily smoothed the observed distribution with a Gaussian with $\sigma_B = 15\,000\ {\rm km\,s^{-1}}$ and considered this as the background distribution. We then searched for possible redshift peaks in the signal distribution, computing for each of them the signal to noise ratio defined as $S/N = (S-B)/B^{1/2}$, where S is the number of sources in a velocity interval of fixed width $\Delta V = 2000\ {\rm km\,s^{-1}}$ around the center of each peak candidate and B is the number of background sources in the same interval. Adopting the threshold $S/N \geq 5$ we find 14 peaks. In order to estimate the expected fraction of possibly "spurious" peaks arising from the background fluctuations, we have simulated 10^5 samples of the same size of the observed distribution and randomly extracted from the smoothed background distribution and applied our peak detection method to each simulated sample. With the adopted threshold, the average number of spurious peaks due to background fluctuations is 0.09. Of the simulated samples, 6.6% show one spurious peak, 0.3% show two spurious peaks, and only two simulation (out of 10^5) has three spurious peaks. None of the simulated samples have four or more spurious peaks. The 14 peaks detected in the procedure described above are listed in Table 2, with the mean redshift of the peak, the number of object (N) within $1000\ {\rm km\,s^{-1}}$ from the peak, the S/N threshold, and a short description of the kind of large scale structure defined by visual inspection of the galaxy spatial distribution. We briefly compare our findings those of previous studies:

– The three clusters at $z = 0.53$, 0.67 and 0.73, already seen in the GOODS-FORS2 and K20 surveys are confirmed by the VIMOS redshifts. The peak at $z = 0.077$ seen in Gilli et al. is not detected in the master catalog. We confirm the sheet-like structures observed at $z = 0.219$ in Gilli et al. (2003) and find a structure at redshift marginally lower, $z = 0.339$, than the one at $z = 0.367$ found by Gilli et al. (2003). An additional scale structure is visible at $z = 0.1241$. A cluster-like structure is also visible at $z = 0.9766$, as confirmed by extended X-ray emission reported by Szokoly et al. (2004). We confirm the detection of the concentrated structures at $z = 1.031$, 1.224, and 1.616, already seen in K20 by Cimatti et al. (2003), in the X-ray sample by Gilli et al. (2003), and in the FORS2 sample by Vanzella et al. (2006). We observe

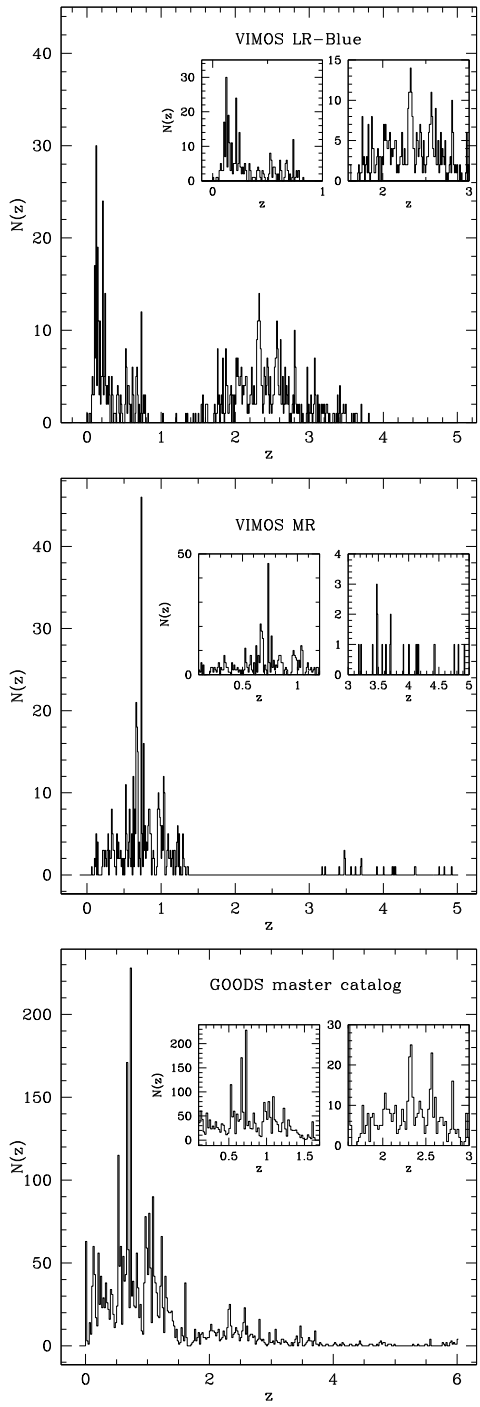

Fig. 9. Fine-grain redshift distribution of the available spectroscopic catalogs: the VIMOS LR-Blue catalog in *the top panel*, the VIMOS MR catalog in the central panel, and the GOODS master catalog in *the bottom panel*. The smaller panels within the main frames show the distribution in redshift regions of particular interest.

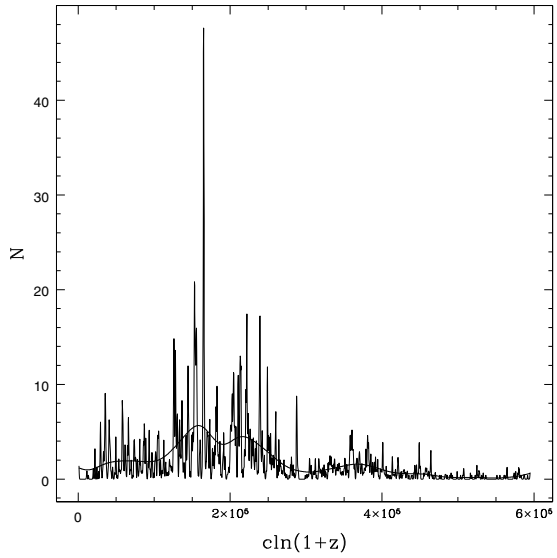

Fig. 10. Galaxy density in velocity space. The solid line is the background distribution obtained by smoothing the observed distribution with a Gaussian with $\sigma_C = 15\,000$ km s^{-1} (solid line). The galaxy distribution is recomputed using $\sigma_S = 300$ km s^{-1} (histogram).

Table 2. Peaks detected in the master catalog redshift distributions, sorted by increasing redshift. The signal and background distribution are smoothed with $\sigma_S = 300$ km s^{-1} and $\sigma_B = 15\,000$ km s^{-1}, respectively. The mean redshift of each peak, the number of sources N within 1000 km s^{-1} from each peak, and the type of large scale structure are also indicated.

z	N	S/N	Type
0.1241	37	>5	groups
0.2190	19	>5	sheet-like
0.3393	18	>5	sheet-like
0.5269	26	>5	sheet-like
0.6741	49	>5	filament
0.7355	174	>5	cluster
0.9766	31	>5	cluster
1.0310	21	>5	sheet-like
1.0990	45	>5	cluster/group
1.2240	48	>5	cluster/group
1.3060	13	>5	cluster/group
1.6160	13	>5	group
2.3160	8	>4.5	sheet-like
2.5600	7	>4.5	sheet-like

additional significant peaks at $z = 1.0990$ and 1.3060, also seen by Adami et al. (2005) and Vanzella et al. (2006);
– we note that other two peaks are been detected with $S/N \sim 4.5$ at $z = 2.316$ and 2.560. The latter peak has also been reported by Gilli et al. (2003). In both cases, the galaxy within 1000 km s^{-1} from the peak occupy the whole GOODS region in a sheet-like structure. The mean projected distance between galaxies and their nearest neighbors is about 4 Mpc in both cases. The probability to detect spurious peaks arising from the background distribution with a SN equal or greater than $SN \sim 4.5$ is about 10^{-3};
– 124 galaxies are observed in the GOODS master sample in the redshift range $3 < z < 4$. No over-densities are confirmed in the considered redshift range;
– 51 galaxies are observed in the GOODS master sample in the redshift range $4 < z < 5$ and 46 at $z > 5$. No over-densities are confirmed in the considered redshift range.

6. Reliability of photometric techniques for the selection of galaxies at $1 < z < 3$

Many photometric techniques have been proposed to select galaxies at high redshift, particularly at $z > 1.5$. Several of these (BzK, "sub"-U-dropouts, U-, B- and V-dropouts criteria) have been used to select targets for the various GOODS-S spectroscopic surveys. The master redshift catalog described in the

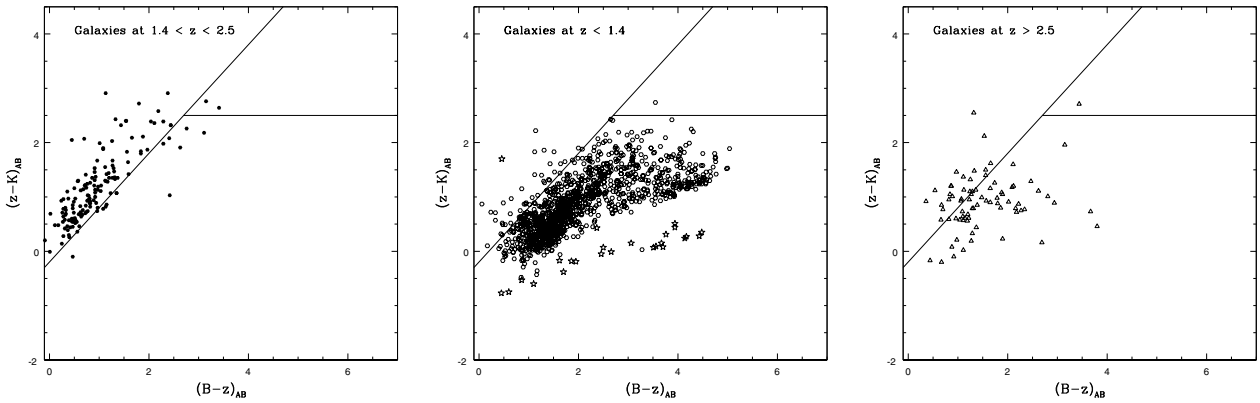

Fig. 11. BzK diagrams of the GOODS-S master catalog. *The left panel* shows all galaxies with redshifts $1.4 < z < 2.5$. *The central panel* shows galaxies with $z < 1.4$ (open circles) and confirmed stars (star symbols), and *the right panel* shows galaxies at $z > 2.5$. The solid lines mark the BzK color selection regions at $(z - K) - (B - z) > 0.2$ and $(z - K) - (B - z) < 0.2, B - z > 2.5$ where the star-forming and passive BzK galaxies, respectively, are expected to lie.

previous section reaches a completeness level >50% at $1.5 < z < 3.5$, and allows us to check the completeness and reliability of different photometric selection techniques by estimating their contamination due to foreground (and background) interlopers outside of the expected redshift ranges for each color selection method.

Figure 11 shows the BzK diagram of Daddi et al. (2004), which aims to select galaxies at $1.4 < z < 2.5$. Spectroscopically confirmed galaxies at $1.4 < z < 2.5$ (left panel), $z < 1.4$ (central panel) and $z > 2.5$ (right panel) are shown in each diagram, along with lines that define the BzK color selection criteria. The PSF-matched photometry of the BzK catalog used in Daddi et al. (2007a,b) has been used to construct these figures. ~86% of galaxies at $1.4 < z < 2.5$ lie in the expected BzK region. 14% of galaxies with redshifts in this range fall outside the BzK color selection window, although most are only slightly outside the expected color ranges, consistent with very modest uncertainties in the photometric measurements. As shown in the central panel, 92% of the galaxies with $z < 1.4$ fall outside the BzK selection region. Again, of the 8% of low redshift galaxies within the BzK area, most are near the color selection boundaries, again consistent with modest photometric errors. The galaxies at $z > 2.5$ are not localized in a specific region of the diagram. Only 27% of those higher redshift objects lie at $(z - K) - (B - z) > 0.2$, and the remaining 73% are located in the same color-color region as the low redshift galaxies. This is expected because at $z > 2.5$ the Lyman forest starts to enter the B band, producing a redder $B - z$ color. To estimate the contamination due to low redshift galaxies in the BzK selection, we examine the redshift distributions of galaxies within and outside the BzK color selection regions. For galaxies within the color selection region for star-forming BzK galaxies, 67% of the sample lie at $1.4 < z < 2.5$, 10% at $z > 2.5$, and the contamination of low redshift interlopers is 23% (see the left panel of Fig. 13). In the BzK passive galaxy region there are only 4 galaxies. 2 of them are at $1.4 < z < 2.5$, one is at $z > 2.5$ and one has $z < 1.4$. We note that the B-band data used for the color measurements is not as deep as would be required to robustly identify passive BzK galaxies, which have extremely red $B - z$ colors. When the same analysis is carried out adopting a brighter magnitude limit, $23 < i < 23.5$, the results are unchanged. Our estimate of the BzK foreground contamination is higher than the 8% fraction found by Daddi et al. (2007a). The difference is largely due to the fact that the latter work excluded from the analysis hard X-ray sources and blended galaxies. AGN contamination of the stellar light from faint galaxies can make them appear redder, and Daddi et al. have found that foreground X-ray sources frequently mimic the redder BzK colors of ordinary galaxies at $z > 1.4$.

We have used the same approach to estimate completeness and contamination of the sub-U-dropout selection criterion. The purpose of this color selection method is to select UV-bright, star-forming galaxies in the redshift range $1.4 < z < 3$. This criterion aims to be similar to the BM/BX selection method proposed by Adelberger et al. (2004). The BM/BX selection method is based on selecting galaxies on the basis of their colors in the $U_n - G$, $G - R_s$ color color diagram. No U_nGR_s photometry is available for the CDF-S, so we have used the $U - B$ and $B - R$ *WFI* colors to define similar color cuts (see Nonino et al. in preparation for more details). The sub-U-dropouts criteria are:

$$U - B > 0.3$$

$$U - B > B - R - 0.3$$

$$B - R < 1.1$$

$$R > 23$$

and not meeting the standard U-drop criterion. The U-dropout criteria are:

$$U - B > 0.9$$

$$U - B > B - R + 0.4$$

$$B - R < 2$$

$$R > 23.$$

Figure 12 shows the $U - B$ and $B - R$ color color diagram for galaxies with measured redshifts $1.4 < z < 3$ (left panel), $z < 1.4$ (central panel) and $z > 3$ (right panel), respectively. The sub-U-dropout color window is located below the U-dropout color limits (thus, the name "sub"-U-dropouts). It is bounded by the solid and the dashed lines showed in the diagrams of Fig. 12. The U-dropouts lie in the area enclosed by the dashed line. As shown in the left panel of the figure, most (80%) of the galaxies at $1.4 < z < 3$ lie in the the sub-U-dropout color selection region, with 8% in the U-drop color region. Most galaxies at $z < 1.4$ (92%) do not lie in the sub-U-dropouts and U-dropouts loci, as

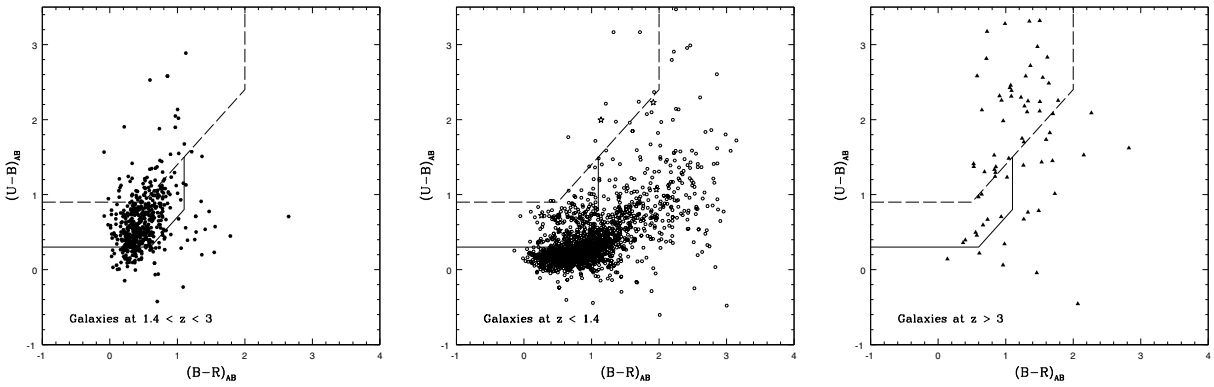

Fig. 12. $U-B-B-R$ color−color diagrams of the GOODS-S master catalog. *The left panel* shows the galaxies at $1.4 < z < 3$, *the central panel* shows the low redshift galaxies ($z < 1.4$), and *the right panel* shows the galaxies at $z > 3$. In *the central panel*, the empty circles refer to the low redshift galaxies and the stars refer to stars. The region comprised between the solid and the dashed lines is the sub-U-dropout locus. The U-dropouts lie above the dashed line.

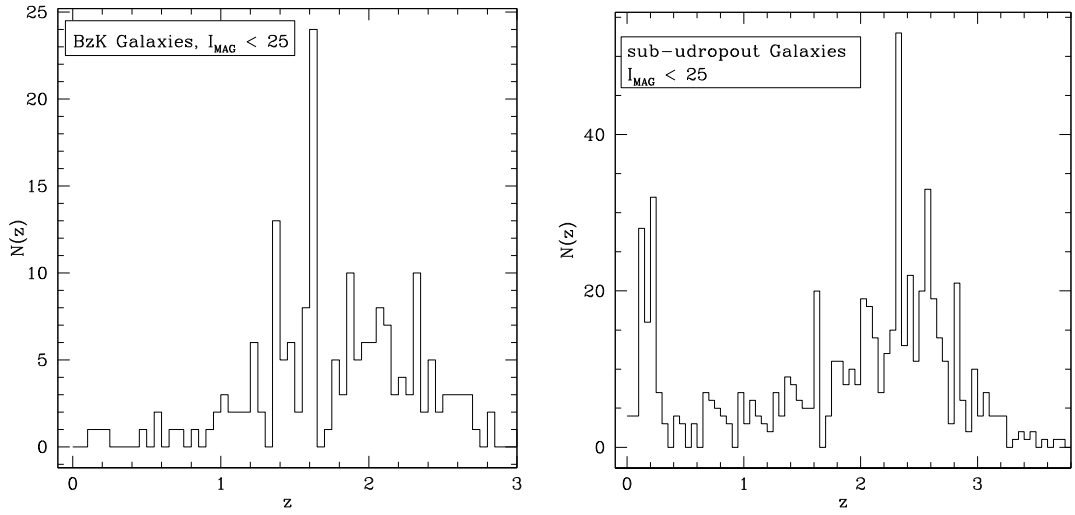

Fig. 13. Redshift distribution of the BzK-selected (*left panel*) and sub-U-dropout (*right panel*) galaxies.

shown in the central panel. 58% of the galaxies at $z > 3$ lie in the U-dropout region and 16% in the sub-U-dropout region (left panel). We have estimated the contamination of the sub-U-drop criterion in a manner analogous to that which we used to test the BzK method. 72% of the sub-U-dropouts candidates at $R > 23$ turn out to be at $1.4 < z < 3$, with a 24% contamination of low redshift objects ($z < 1.4$) and a remaining 4% of higher redshift objects ($z > 3$) (see also the right panel of Fig. 13). In particular, there is a peak of galaxies at $z \sim 0.2$ whose colors fall within the sub-U-dropout selection region. The fractional contamination by low redshift galaxies is similar to that of the BzK selection method and it is consistent with the results obtained by Adelberger et al. (2004). We have done the same exercise for the U-dropout (as defined above) and the B- and V-dropout selection method (as defined in Giavalisco et al. 2004). In all three cases the LBG technique provides galaxy samples in the desired redshift range with a ∼80% completeness and a ∼25% contamination by lower redshift galaxies.

7. Conclusions

We have observed a large sample of galaxies in the Chandra Deep Field South with the VIMOS spectrograph on the VLT, as part of a public campaign of ESO spectroscopy for the Great Observatories Origins Deep Survey southern field. A total of 3312 objects with $i_{775} \lesssim 25$ has been observed with the VIMOS LR-Blue and MR grisms, providing 2137 redshift measurements. From a variety of diagnostics the measurement of the redshifts appears to be accurate (with a typical $\sigma_z = 0.001$) and reliable. The reliability of the redshift estimate varies with the quality flag. VIMOS LR-Blue quality flag A redshifts are reliable at 93−95% confidence level, flag B redshidts at 60−80% and quality C et 30−50%. In the MR case, quality flag A redshifts are reliable at 100% confidence level, quality B at 80−95% and quality C $z_{\rm spec}$ at 60−75%. The confidence level ranges are determined in all cases by comparing our redshift estimates with estimates provided by different spectroscopic surveys and photometeric redshift catalogs. The spectroscopic coverage of the CDF-S achieved by combining the VIMOS spectroscopic sample with other redshifts available from the literature is very high, ∼60% up to redshift $z \sim 3.5$. It is more uncertain at higher redshifts. A "master catalog" combining the VIMOS redshifts presented in this paper and other, large samples available in the literature have been used to test the accuracy of the BzK, sub-U-dropout color selection techniques. We show that any of these methods permits the selection of high redshift galaxies with a contamination of ∼25% of low redshift sources and a completeness level of 80%. We also identify several large scale structures in the GOODS region.

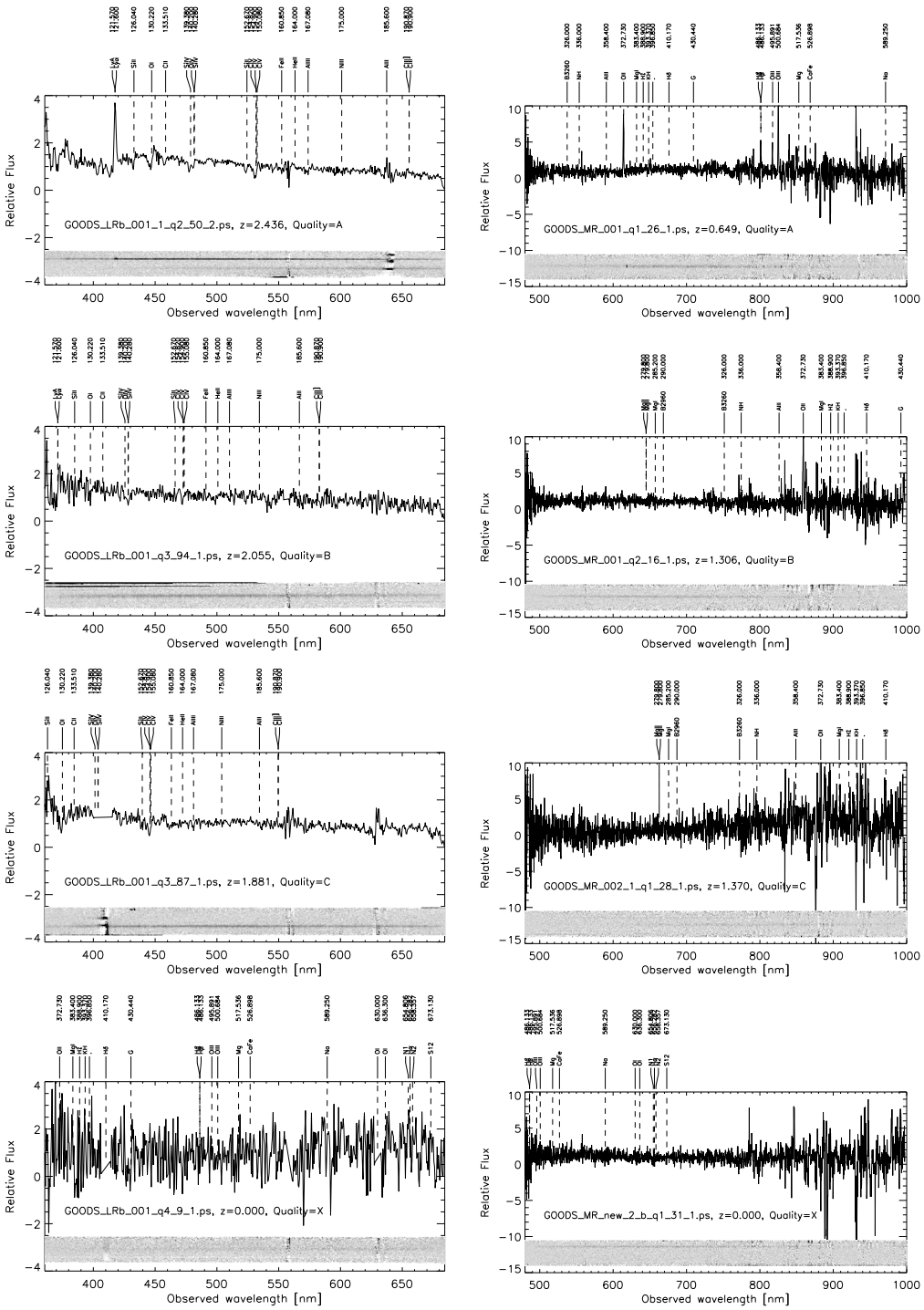

Fig. A.1. Examples of spectra with redshift estimates of different quality. *The left column* of the figure illustrates 1D and 2D spectra observed with the VIMOS LR-Blue grism with redshift of quality flag A, B, C and X. *The right column* shows the same examples for the MR grism.

The reduced spectra and the derived redshifts have been released to the community (http://archive.eso.org/cms/eso-data/data-packages). They constitute an essential contribution to achieve the scientific goals of GOODS, providing the time coordinate needed to delineate the evolution of galaxy properties, morphologies, and star formation and to underhand the galaxy mass assembly.

Acknowledgements. We are grateful to the ESO staff in Paranal and Garching who greatly helped in the development of this program. We would like to thank Martino Romaniello and Carlo Izzo for many stimulating discussions and for the help in reducing the VIMOS data. We would like to thank also Remco Slijkhuis and Joerg Retzlaff for their work on VIMOS/GOODS release.

Appendix A: Spectra quality flags

Figure A.1 shows examples of spectra with redshift estimates of different quality. The left column of the figure illustrates 1D and 2D spectra observed with the VIMOS LR-Blue grism with redshift of quality flag A, B, C and X. The right column shows the same examples for the MR grism. Quality A spectra (first two panels) show clear emission and absorption features. Quality B

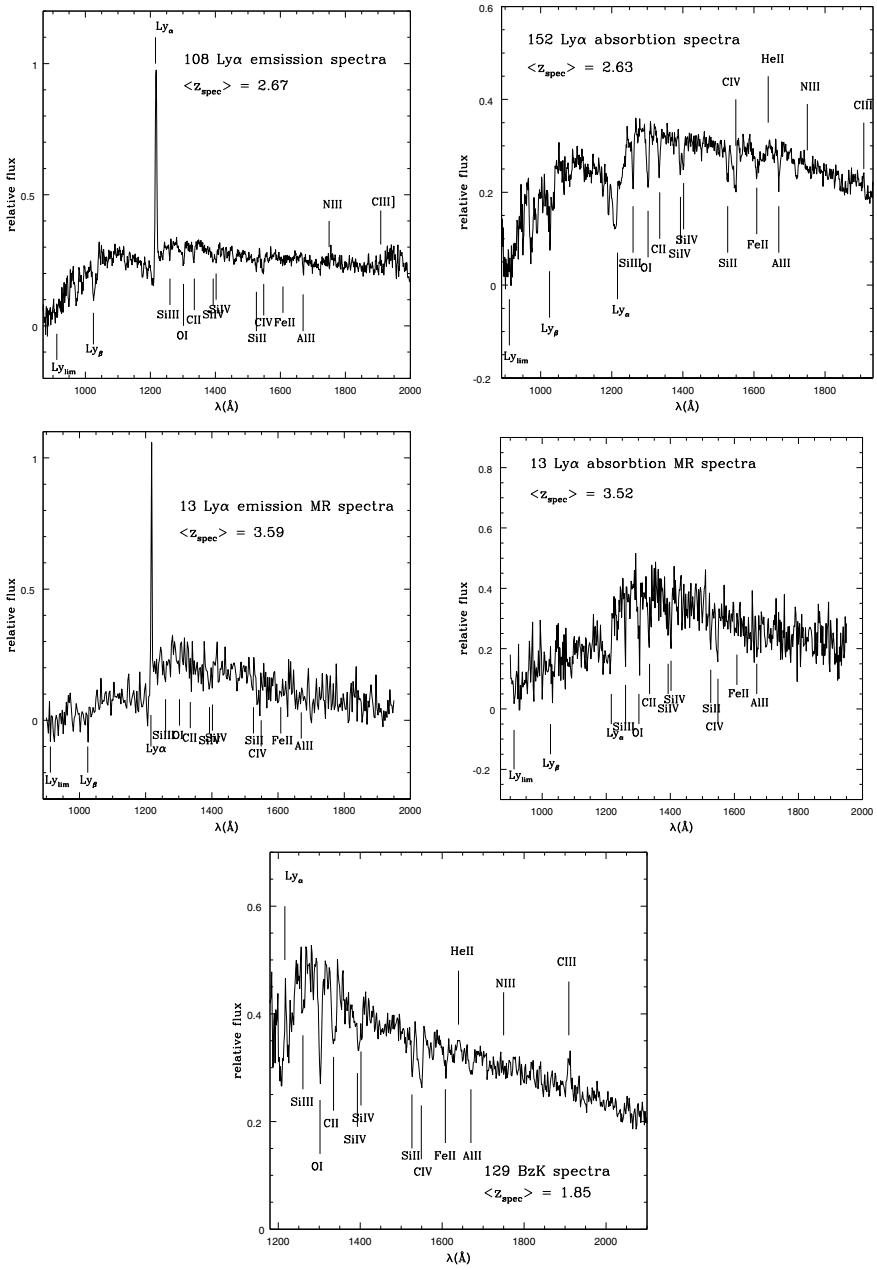

Fig. B.1. Combined 1D spectra of high redshift galaxies in different redshift bins. *The top panels* show LBGs with the Lyα in emission (*left panel*) and in absorption (*right panel*) obtained with the LR-Blue grism at $z \sim 2.6$. The *central panels* show LBGs with the Lyα in emission (*left panel*) and in absorption (*right panel*) obtained with the MR grism at $z \sim 3.5$. The *bottom panel* shows the combined 1D spectrum of a BzK galaxy obtained with the LR-Blue grism at $z \sim 1.85$.

spectra (second row of the Fig. A.1) show clear emission and absorption features but with somewhat lower quality: Lyα absorption at the edge of the spectrum in the LR-Blue spectrum (left panel), strong [OII] emission in the fringing area in the MR spectrum (right panel). The C quality spectra (third row of the Fig. A.1) show only marginally significant features: only OI and CIV absorption in the LR-Blue spectrum (left panel) and faint [OII] emission in the fringing region of the MR spectrum (right panel). The quality X spectra (last row of the Fig. A.1) do not show any emission or absorption features.

Appendix B: Spectra templates

Figure B.1 shows several templates of the high redshift galaxies observed during the GOODS-VIMOS spectroscopic campaign. The templates have been obtained by stacking the 1D rest-frame spectra. The first row of the figure show the Lyα emission (left panel) and absorption (right panel) galaxies at $z \sim 2.6$ obtained by stacking ~150 LR-Blue spectra. The second row of the figure shows Lyα emission (left panel) and absorption (right panel) galaxies at $z \sim 3.5$ obtained by stacking in both cases 13 MR spectra. The last row shows a template of BzK spectrum at $z \sim 1.8$. All the emission and absorption features used to identify the spectroscopic redshifts are outlined in the individual panels.

References

Adami, C., Mazure, A., & Ilbert, O. 2005, A&A, 443, 805
Adelberger, K. L., Steidel, C. C., Shapley, A. E., et al. 2004, ApJ, 607, 226

Bottini, D., Garilli, B., Maccagni, D., et al. 2005, PASP, 117, 996
Cimatti, A., Mignoli, M., Daddi, E., et al. 2002, A&A, 392, 395
Cohen, J. G., Blandford, R., Hogg, D. W., et al. 1999, ApJ, 512,30
Daddi, E., Cimatti, A., Renzini, A., et al. 2004, ApJ, 617, 746
Daddi, E., Alexander, D. M., Dickinson, M., et al. 2007a, ApJ, 670, 173
Daddi, E., Dickinson, M., Morrison, G., et al. 2007b, ApJ, 670, 156
Dickinson, M., Giavalisco, M., & The Goods Team 2003, in The Mass of Galaxies at Low and High Redshift: Proc. of the ESO/USM Workshop (Venice, Italy, October 2001), ed. R. Bender, & A. Renzini, 324
Giacconi, R., Zirm, A., Wang, J., et al. 2002, ApJS, 139, 369
Giavalisco, M., Ferguson, H. C., Koekemoer, A. M., et al. 2004, ApJ, 600, L93
Gilli, R., Cimatti, A., Daddi, E., et al. 2003, ApJ, 592, 721
Grazian, A., Fontana, A., de Santis, C., et al. 2006, A&A, 449, 951
Horne, K. 1986, PASP, 98, 609
Kirby, E. N., Guhathakurta, P., Faber, S. M., et al. 2007, ApJ, 660, 62
Kurtz, M. J., & Mink, D. J. 1998, PASP, 110, 934
Lee, K. S., Giavalisco, M., Gnedin, O. Y., et al. 2006, ApJ, 642, 63
Le Fevre, O., Vettolani, G., Maccagni, D., et al. 2003, SPIE, 4834, 173
Le Fevre, O., Vettolani, G., Paltani, S., et al. 2005, A&A, 428, 1043
Lehmer, B. D., Brandt, W. N., Alexander, D. M., et al. 2005, ApJS, 161, 21
Ravikumar, C. D., Puech, M., Flores, H., et al. 2007, A&A, 465, 1099
Renzini, A., Cesarsky, C., Cristiani, S., et al. 2003, in The Mass of Galaxies at Low and High Redshift: Proc. of the ESO/USM Workshop (Venice, Italy, October 2001), ed. R. Bender, & A. Renzini, 332
Scodeggio, M., Franzetti, P., Garilli, B., et al. 2005, PASP, 117, 1284
Szokoly, G. P., Bergeron, J., Hasinger, G., et al. 2004, ApJS, 155, 271
Vanzella, E., Cristiani, S., Dickinson, M., et al. 2005, A&A, 434, 53
Vanzella, E., Cristiani, S., Dickinson, M., et al. 2006, A&A, 454, 423
Vanzella, E., Cristiani, S., Dickinson, M., et al. 2008, A&A, 478, 83
Warmels, R. H. 1991, The ESO-MIDAS System, in Astronomical Data Analysis Software and Systems I, PASP Conf. Ser., 25, 115